

I $\kappa$ B degradation. Taking these observations together, although PKC $\theta$ -mediated NF- $\kappa$ B activation via palmitate-induced intracellular lipid accumulation has been implicated in the increased secretion of IL-6 and TNF $\alpha$  (9, 29, 30, 53), our present data provide compelling evidence that p38 MAPK, but not PKC $\theta$ , serves as the crucial signaling intermediate for the COX-2 expression in C<sub>2</sub>C<sub>12</sub> skeletal muscle cells. A similar mechanism was also observed for the palmitate-induced suppression of PGC-1 $\alpha$  expression in skeletal muscle cells (10, 11).

*Mitochondrial overload, ceramide, and Toll-like receptors do not play a crucial role in palmitate-induced COX-2 expression.* An interesting observation reported herein is that inhibition of fatty acid oxidation by various reagents that modulate mitochondrial respiration and reactive oxygen species (ROS) generation totally failed to influence palmitate-induced COX-2 expression (Fig. 5), which would appear to contradict a recent report showing that mitochondrial overload with excessive  $\beta$ -oxidation could be a major cause of insulin resistance in skeletal muscle (36). Because 1 mM of a halogenated analog of palmitate, 2-BP (22), has no COX-2-inducible effect, a specific fatty acyl-CoA moiety and/or palmitate metabolism is apparently required for COX-2 expression (Fig. 5). In addition, it has been reported that mitochondria-derived ROS is a key initiator for the

phosphorylation of p38 (37). Since we have not examined the effects of supplemental carnitine, which reportedly tends to be deficient in cell cultures and thereby partially obliterates actual mitochondrial performance (36), we cannot as yet exclude the involvement of mitochondrial ROS generation in palmitate-induced COX-2 expression. Elucidation of this possibility requires further experiments.

Although it has been reported that palmitate can activate the proinflammatory pathway via a Toll-like receptor-dependent mechanism(s) (12, 51), we observed no inhibitory effects of blocking antibodies against Toll-like receptor-2/4 on palmitate-induced COX-2 expression (data not shown). We also examined the possible involvement of ceramide in COX-2 expression by utilizing a cell-permeable C2-ceramide (50). However, 100  $\mu$ M C2-ceramide did not induce COX-2 expression in C<sub>2</sub>C<sub>12</sub> myotubes (data not shown), indicating ceramide itself to be insufficient for reproducing palmitate-induced COX-2 expression, although ceramide accumulation might contribute to this event in conjunction with other palmitate-induced component(s).

*Effects of unsaturated FFAs on COX-2 expression and intracellular signals evoked by palmitate treatment.* Although a recent report proposed the importance of palmitoleate (16:1) serving as an adipose-derived lipid hormone (lipokine) (5), our findings indicate that palmitoleate, in contrast

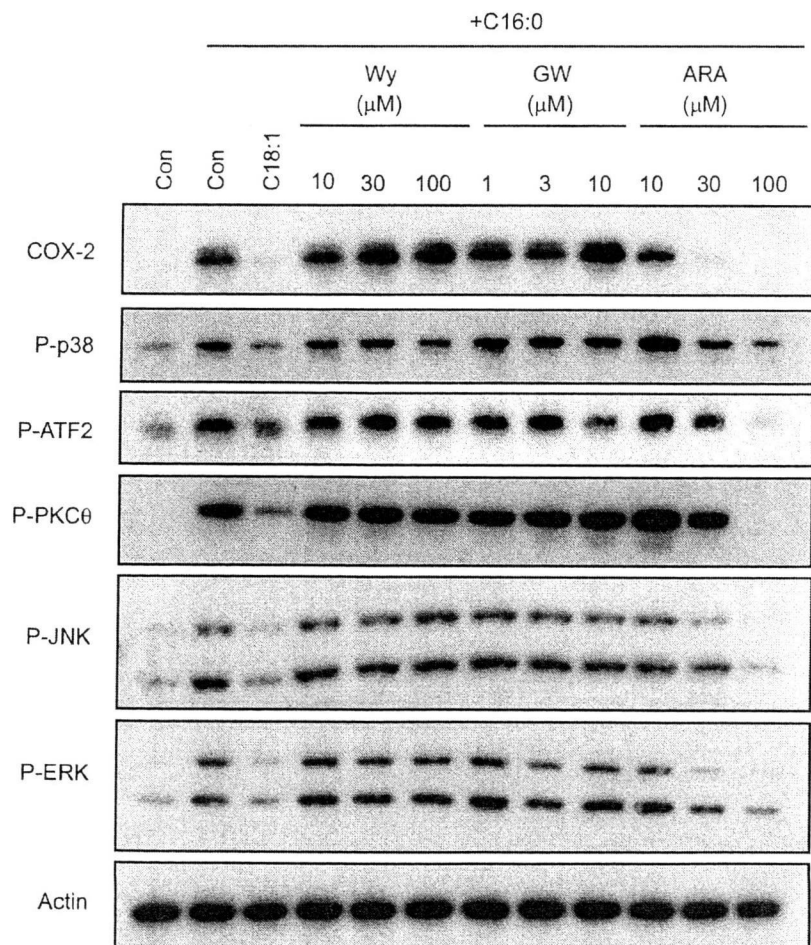


Fig. 7. Effects of Wy-14643 (Wy), GW-50156 (GW), and arachidonate (ARA) on palmitate-induced COX-2 expression and its signaling pathways. C<sub>2</sub>C<sub>12</sub> myotubes were treated with 1 mM palmitate (C16:0) alone or in combination with 300 mM oleate (C18:1) and several concentrations of Wy, GW, or ARA for 16 h. The cell lysates were then subjected to Western blot analysis. Three independent experiments were performed, and representative results were obtained. ATF-2, activating transcription factor-2.

to oleate (18:1) and linoleate (18:2), has relatively fewer beneficial effects in terms of suppressing COX-2 expression as well as having little impact on the intracellular signals evoked by palmitate treatment (Fig. 6). These observations are quite novel and raise an important question concerning the significance of palmitoleate serving as a lipokine, at least in terms of exerting protective effects against the COX-2 expression triggered by palmitate treatment in skeletal muscle cells. Given that the serum palmitoleate concentration is usually quite low, and oleate and linoleate are the most prevalent unsaturated FFAs in the circulation (7), our results suggest oleate and/or linoleate, but not palmitoleate, to potentially be major contributors to the protective effects against palmitate-induced COX-2 expression in vivo via dampening of a wide array of the palmitate-inducible intracellular signaling cascades (Fig. 6).

It is well established that unsaturated FFAs function as ligands for PPARs, including PPAR $\beta/\delta$ , a predominant skeletal muscle PPAR isoform, with different binding affinities (16). For example, oleate (18:1) has recently been shown to provide protection from palmitate-induced detrimental responses by promoting mitochondrial  $\beta$ -oxidation as well as by shunting excess palmitate to triacylglycerol instead of diacylglycerol accumulation through a mechanism involving a PPAR $\alpha$ -dependent upregulation of the related metabolic genes, which in turn results in the prevention of inappropriate activation of the PKC $\theta$ -NF- $\kappa$ B cascades in skeletal muscle cells (9). We also observed the palmitate-induced phosphorylation of PKC $\theta$  to be inhibited by each unsaturated FFA examined (Fig. 6). However, in contrast to this notion, we could not reproduce the protective action against palmitate-induced events using a selective PPAR $\beta/\delta$  activator, GW-50156, or a PPAR $\alpha$  activator, Wy-140143 (Fig. 7), suggesting that PPARs may not be a major contributor to the protective actions. Consistent with this, neither Wy-14643 nor GW-50156 had any suppressive effect on palmitate-induced phosphorylation of PKC $\theta$  (Fig. 7). Since arachidonate (20:4), a polyunsaturated fatty acid serving as a major substrate for COXs, has also been shown to potentially activate both PPAR $\alpha$  and PPAR $\beta/\delta$  (16), we utilized arachidonate as an endogenous pan-PPAR agonist. Unexpectedly, arachidonate strongly suppressed palmitate-induced events (Fig. 7), raising the possibility that arachidonate and its metabolite(s) play an important role in exerting the protective actions. In line with this, linoleate, which is preferentially metabolized to arachidonate, exhibited a stronger suppressive effect on palmitate-induced events than oleate or palmitoleate (Fig. 6). Together, these observations suggest a potential role for the arachidonate cascade, including synthesis of bioactive lipids in the protective actions of unsaturated FFAs.

*p38 Phosphorylation induced by palmitate in combination with unsaturated FFAs shows a bell-shaped dose-response relationship.* Our data demonstrated that p38 MAPK is required for COX-2 expression and that unsaturated FFAs potentially abolished this palmitate-induced COX-2 expression. Intriguingly, however, we found that all three unsaturated FFAs similarly induced slight enhancement of palmitate-induced p38 phosphorylation (Thr<sup>180</sup>/Tyr<sup>182</sup>), showing a bell-shaped dose-response relationship (Fig. 6C), whereas they all diminished the phosphorylations of JNKs (Fig. 6, F and G) and ATF-2 (Fig. 6E), a common substrate for p38 and JNK

MAPKs (21). This discrepancy between the phosphorylation status of p38 MAPK (Thr<sup>180</sup>/Tyr<sup>182</sup>) and its substrate ATF-2 (Thr<sup>69/71</sup>) (Fig. 6D) apparently reflects the complex regulatory mechanism of p38 by multiple phosphorylation events and by

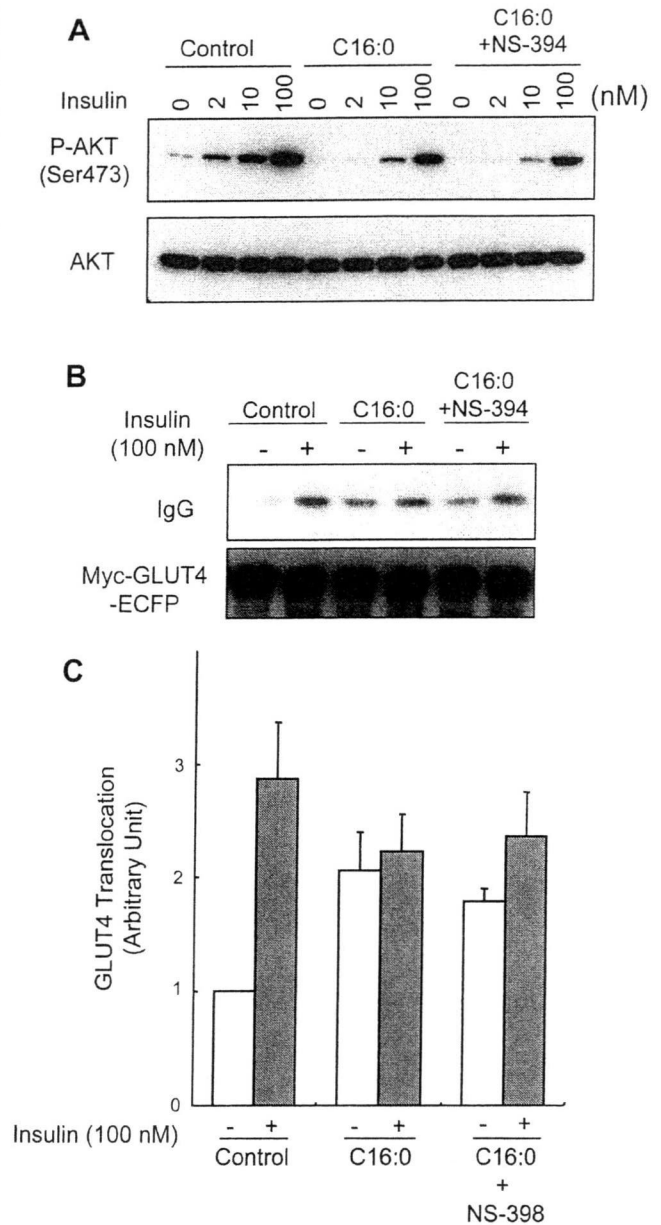


Fig. 8. Effects of NS-398 on palmitate-induced insulin resistance. *A*: C<sub>2</sub>C<sub>12</sub> myotubes were treated with 1 mM palmitate (C16:0) alone or in combination with 30  $\mu$ M NS-398 for 16 h. The cells were serum-starved and then treated with the indicated concentration of insulin for 5 min. The cell lysates were then subjected to Western blot analysis using anti-phospho Akt (Ser<sup>473</sup>) or anti-Akt antibodies. *B*: differentiated C<sub>2</sub>C<sub>12</sub> myotubes expressing myc-glucose transporter 4 (GLUT4)-enhanced cyan fluorescent protein (ECFP) were treated with 100 nM insulin for 30 min in the presence of 4  $\mu$ g/ml anti-myc antibody. The cells were then washed 5 times with PBS and analyzed by Western blotting with the use of anti-mouse IgG horseradish peroxidase-conjugated antibody. *C*: the results from *B*, uptake of anti-myc antibody in response to insulin, were subjected to densitometric analysis for quantification. Three independent experiments were performed, and representative results were obtained.

binding of unsaturated FFAs or their metabolites (e.g., arachidonate) to the lipid-binding site of this enzyme (14, 44, 48). Thus, an interesting aspect of unsaturated FFA actions on p38 regulation might be further involvement in the beneficial effects of suppressing inflammatory responses.

**Potential role of COX-2 and subsequent PG production in skeletal muscle.** Although palmitate treatment clearly induced PGE<sub>2</sub> production in C<sub>2</sub>C<sub>12</sub> myotubes (Figs. 2F and 6J), NS-398, a COX-2-selective inhibitor, failed to reverse the palmitate-induced impairments in both insulin-induced Akt phosphorylation and insulin-responsive GLUT4 translocation (Fig. 8). These data indicate that palmitate-induced COX-2 and its metabolites may make little, if any, direct contribution to the development of insulin resistance in C<sub>2</sub>C<sub>12</sub> myotubes. However, it is highly likely that COX-2 metabolites are involved in inflammatory responses in a paracrine fashion by inducing migration of immune cells (13, 27, 38, 47), which may contribute indirectly to the generation of insulin resistance as well as to complex inflammatory responses in skeletal muscles *in vivo*. In this regard, a recent study demonstrated that administration of a COX-2 inhibitor improved whole body and muscle insulin resistance in sucrose-fed rats (28). In addition, recent studies utilizing COX-2-deficient mice have also demonstrated that COX-2 plays a crucial role in the regeneration of injured muscle (2) and growth of atrophied muscle (3), indicating that inflammation, induced at least in part by COX-2-mediated PG production, is an important process of skeletal muscle healing. Analogous to this, our results indicate that inducible expression of COX-2 and subsequent PGE<sub>2</sub> production may contribute to muscle healing/regeneration after cell damage caused by treatment with pathophysiologically high FFA concentrations.

#### ACKNOWLEDGMENTS

We thank Fumie Wagatsuma and Natsumi Emoto for their technical assistance.

#### GRANTS

This study was supported by Special Coordination Funds for Promoting Science and Technology and also in part by grants from the Ministry of Education, Science, Sports, and Culture of Japan and the New Energy and Industrial Technology Development Organization.

#### DISCLOSURES

No conflicts of interest are declared by the author(s).

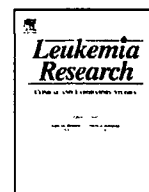
#### REFERENCES

- Belfort R, Mandarino L, Kashyap S, Wirfel K, Pratipanawatr T, Berria R, DeFronzo RA, Cusi K. Dose-response effect of elevated plasma free fatty acid on insulin signaling. *Diabetes* 54: 1640–1648, 2005.
- Bondesen BA, Mills ST, Kegley KM, Pavlath GK. The COX-2 pathway is essential during early stages of skeletal muscle regeneration. *Am J Physiol Cell Physiol* 287: C475–C483, 2004.
- Bondesen BA, Mills ST, Pavlath GK. The COX-2 pathway regulates growth of atrophied muscle via multiple mechanisms. *Am J Physiol Cell Physiol* 290: C1651–C1659, 2006.
- Burleigh ME, Babaev VR, Yancey PG, Major AS, McCaleb JL, Oates JA, Morrow JD, Fazio S, Linton MF. Cyclooxygenase-2 promotes early atherosclerotic lesion formation in ApoE-deficient and C57BL/6 mice. *J Mol Cell Cardiol* 39: 443–452, 2005.
- Cao H, Gerhold K, Mayers JR, Wiest MM, Watkins SM, Hotamisligil GS. Identification of a lipokine, a lipid hormone linking adipose tissue to systemic metabolism. *Cell* 134: 933–944, 2008.
- Chavez JA, Summers SA. Characterizing the effects of saturated fatty acids on insulin signaling and ceramide and diacylglycerol accumulation in 3T3-L1 adipocytes and C2C12 myotubes. *Arch Biochem Biophys* 419: 101–109, 2003.
- Clore JN, Allred J, White D, Li J, Stillman J. The role of plasma fatty acid composition in endogenous glucose production in patients with type 2 diabetes mellitus. *Metabolism* 51: 1471–1477, 2002.
- Coleman RA, Rao P, Fogelsson RJ, Bardes ES. 2-Bromopalmitoyl-CoA and 2-bromopalmitate: promiscuous inhibitors of membrane-bound enzymes. *Biochim Biophys Acta* 1125: 203–209, 1992.
- Coll T, Eyre E, Rodriguez-Calvo R, Palomer X, Sanchez RM, Merlos M, Laguna JC, Vazquez-Carrera M. Oleate reverses palmitate-induced insulin resistance and inflammation in skeletal muscle cells. *J Biol Chem* 283: 11107–11116, 2008.
- Coll T, Jove M, Rodriguez-Calvo R, Eyre E, Palomer X, Sanchez RM, Merlos M, Laguna JC, Vazquez-Carrera M. Palmitate-mediated down-regulation of peroxisome proliferator-activated receptor-gamma coactivator 1alpha in skeletal muscle cells involves MEK1/2 and nuclear factor-kappaB activation. *Diabetes* 55: 2779–2787, 2006.
- Crunkhorn S, Dearie F, Mantzoros C, Gami H, da Silva WS, Espinoza D, Faucette R, Barry K, Bianco AC, Patti ME. Peroxisome proliferator activator receptor gamma coactivator-1 expression is reduced in obesity: potential pathogenic role of saturated fatty acids and p38 mitogen-activated protein kinase activation. *J Biol Chem* 282: 15439–15450, 2007.
- Davis JE, Gabler NK, Walker-Daniels J, Spurlock ME. Tlr-4 deficiency selectively protects against obesity induced by diets high in saturated fat. *Obesity (Silver Spring)* 16: 1248–1255, 2008.
- de Menezes GB, dos Reis WG, Santos JM, Duarte ID, de Francischi JN. Inhibition of prostaglandin F(2alpha) by selective cyclooxygenase 2 inhibitors accounts for reduced rat leukocyte migration. *Inflammation* 29: 163–169, 2005.
- Diskin R, Engelberg D, Livnah O. A novel lipid binding site formed by the MAP kinase insert in p38 alpha. *J Mol Biol* 375: 70–79, 2008.
- Fain JN, Ballou LR, Bahouth SW. Obesity is induced in mice heterozygous for cyclooxygenase-2. *Prostaglandins Other Lipid Mediat* 65: 199–209, 2001.
- Forman BM, Chen J, Evans RM. Hypolipidemic drugs, polyunsaturated fatty acids, and eicosanoids are ligands for peroxisome proliferator-activated receptors alpha and delta. *Proc Natl Acad Sci USA* 94: 4312–4317, 1997.
- Funk CD. Prostaglandins and leukotrienes: advances in eicosanoid biology. *Science* 294: 1871–1875, 2001.
- Gilroy DW, Colville-Nash PR, Willis D, Chivers J, Paul-Clark MJ, Willoughby DA. Inducible cyclooxygenase may have anti-inflammatory properties. *Nat Med* 5: 698–701, 1999.
- Griffin ME, Marcucci MJ, Cline GW, Bell K, Barucci N, Lee D, Goodyear LJ, Kraegen EW, White MF, Shulman GI. Free fatty acid-induced insulin resistance is associated with activation of protein kinase C theta and alterations in the insulin signaling cascade. *Diabetes* 48: 1270–1274, 1999.
- Guilherme A, Virbasius JV, Puri V, Czech MP. Adipocyte dysfunctions linking obesity to insulin resistance and type 2 diabetes. *Nat Rev Mol Cell Biol* 9: 367–377, 2008.
- Gupta S, Campbell D, Derijard B, Davis RJ. Transcription factor ATF2 regulation by the JNK signal transduction pathway. *Science* 267: 389–393, 1995.
- Hagve TA, Christophersen BO. In vitro effects of alpha-bromopalmitate on metabolism of essential fatty acids studied in isolated rat hepatocytes: sex differences. *Biochim Biophys Acta* 917: 333–336, 1987.
- Hisatsune J, Yamasaki E, Nakayama M, Shirasaka D, Kurazono H, Katagata Y, Inoue H, Han J, Sap J, Yahiro K, Moss J, Hirayama T. Helicobacter pylori VacA enhances prostaglandin E2 production through induction of cyclooxygenase 2 expression via a p38 mitogen-activated protein kinase/activating transcription factor 2 cascade in AZ-521 cells. *Infect Immun* 75: 4472–4481, 2007.
- Hommelberg PP, Plat J, Langen RC, Schols AM, Mensink RP. Fatty acid-induced NF-κB activation and insulin resistance in skeletal muscle are chain length dependent. *Am J Physiol Endocrinol Metab* 296: E114–E120, 2009.
- Horsley V, Pavlath GK. Prostaglandin F2(alpha) stimulates growth of skeletal muscle cells via an NFATC2-dependent pathway. *J Cell Biol* 161: 111–118, 2003.
- Hotamisligil GS. Inflammation and metabolic disorders. *Nature* 444: 860–867, 2006.

27. Hsieh PS, Jin JS, Chiang CF, Chan PC, Chen CH, Shih KC. COX-2-mediated inflammation in fat is crucial for obesity-linked insulin resistance and fatty liver. *Obesity (Silver Spring)* 17: 1150–1157, 2009.
28. Hsieh PS, Tsai HC, Kuo CH, Chan JY, Shyu JF, Cheng WT, Liu TT. Selective COX2 inhibition improves whole body and muscular insulin resistance in fructose-fed rats. *Eur J Clin Invest* 38: 812–819, 2008.
29. Jové M, Planavila A, Laguna JC, Vázquez-Carrera M. Palmitate-induced interleukin 6 production is mediated by protein kinase C and nuclear-factor kappaB activation and leads to glucose transporter 4 down-regulation in skeletal muscle cells. *Endocrinology* 146: 3087–3095, 2005.
30. Jové M, Planavila A, Sánchez RM, Merlos M, Laguna JC, Vázquez-Carrera M. Palmitate induces tumor necrosis factor-alpha expression in C2C12 skeletal muscle cells by a mechanism involving protein kinase C and nuclear factor-kappaB activation. *Endocrinology* 147: 552–561, 2006.
31. Karamouzis M, Langberg H, Skovgaard D, Bülow J, Kjaer M, Saltin B. In situ microdialysis of intramuscular prostaglandin and thromboxane in contracting skeletal muscle in humans. *Acta Physiol Scand* 171: 71–76, 2001.
32. Kellogg AP, Wiggin TD, Larkin DD, Hayes JM, Stevens MJ, Pop-Busui R. Protective effects of cyclooxygenase-2 gene inactivation against peripheral nerve dysfunction and intraepidermal nerve fiber loss in experimental diabetes. *Diabetes* 56: 2997–3005, 2007.
33. Kiritoshi S, Nishikawa T, Sonoda K, Kukidome D, Senokuchi T, Matsuo T, Matsumura T, Tokunaga H, Brownlee M, Araki E. Reactive oxygen species from mitochondria induce cyclooxygenase-2 gene expression in human mesangial cells: potential role in diabetic nephropathy. *Diabetes* 52: 2570–2577, 2003.
34. Kliewer SA, Forman BM, Blumberg B, Ong ES, Borgmeyer U, Mangelsdorf DJ, Umesono K, Evans RM. Differential expression and activation of a family of murine peroxisome proliferator-activated receptors. *Proc Natl Acad Sci USA* 91: 7355–7359, 1994.
35. Koliopoulos A, Friess H, Kleeff J, Roggo A, Zimmermann A, Büchler MW. Cyclooxygenase 2 expression in chronic pancreatitis: correlation with stage of the disease and diabetes mellitus. *Digestion* 64: 240–247, 2001.
36. Kovcs TR, Ussher JR, Noland RC, Slentz D, Mosedale M, Ilkayeva O, Bain J, Stevens R, Dyck JR, Newgard CB, Lopaschuk GD, Muoio DM. Mitochondrial overload and incomplete fatty acid oxidation contribute to skeletal muscle insulin resistance. *Cell Metab* 7: 45–56, 2008.
37. Kulisz A, Chen N, Chandel NS, Shao Z, Schumacker PT. Mitochondrial ROS initiate phosphorylation of p38 MAP kinase during hypoxia in cardiomyocytes. *Am J Physiol Lung Cell Mol Physiol* 282: L1324–L1329, 2002.
38. Menezes GB, Rezende RM, Pereira-Silva PE, Klein A, Cara DC, Francischi JN. Differential involvement of cyclooxygenase isoforms in neutrophil migration in vivo and in vitro. *Eur J Pharmacol* 598: 118–122, 2008.
39. Nedachi T, Fujita H, Kanzaki M. Contractile C<sub>2</sub>C<sub>12</sub> myotube model for studying exercise-inducible responses in skeletal muscle. *Am J Physiol Endocrinol Metab* 295: E1191–E1204, 2008.
40. Nedachi T, Kadotani A, Ariga M, Katagiri H, Kanzaki M. Ambient glucose levels qualify the potency of insulin myogenic actions by regulating SIRT1 and FoxO3a in C<sub>2</sub>C<sub>12</sub> myocytes. *Am J Physiol Endocrinol Metab* 294: E668–E678, 2008.
41. Nedachi T, Kanzaki M. Regulation of glucose transporters by insulin and extracellular glucose in C<sub>2</sub>C<sub>12</sub> myotubes. *Am J Physiol Endocrinol Metab* 291: E817–E828, 2006.
42. Oliver WR Jr, Shenk JL, Snaith MR, Russell CS, Plunket KD, Bodkin NL, Lewis MC, Winegar DA, Sznajdman ML, Lambert MH, Xu HE, Sternbach DD, Kliewer SA, Hansen BC, Willson TM. A selective peroxisome proliferator-activated receptor delta agonist promotes reverse cholesterol transport. *Proc Natl Acad Sci USA* 98: 5306–5311, 2001.
43. Park SW, Sung MW, Heo DS, Inoue H, Shim SH, Kim KH. Nitric oxide upregulates the cyclooxygenase-2 expression through the cAMP-response element in its promoter in several cancer cell lines. *Oncogene* 24: 6689–6698, 2005.
44. Peregrin S, Jurado-Pueyo M, Campos PM, Sanz-Moreno V, Ruiz-Gomez A, Crespo P, Mayor F Jr, Murga C. Phosphorylation of p38 by GRK2 at the docking groove unveils a novel mechanism for inactivating p38MAPK. *Curr Biol* 16: 2042–2047, 2006.
45. Poligone B, Baldwin AS. Positive and negative regulation of NF-kappaB by COX-2: roles of different prostaglandins. *J Biol Chem* 276: 38658–38664, 2001.
46. Pop-Busui R, Marinescu V, Van Huysen C, Li F, Sullivan K, Greene DA, Larkin D, Stevens MJ. Dissection of metabolic, vascular, and nerve conduction interrelationships in experimental diabetic neuropathy by cyclooxygenase inhibition and acetyl-L-carnitine administration. *Diabetes* 51: 2619–2628, 2002.
47. Reding T, Bimmler D, Perren A, Sun LK, Fortunato F, Storni F, Graf R. A selective COX-2 inhibitor suppresses chronic pancreatitis in an animal model (WBN/Kob rats): significant reduction of macrophage infiltration and fibrosis. *Gut* 55: 1165–1173, 2006.
48. Salvador JM, Mittelstadt PR, Guszczynski T, Copeland TD, Yamaguchi H, Appella E, Fornace AJ Jr, Ashwell JD. Alternative p38 activation pathway mediated by T cell receptor-proximal tyrosine kinases. *Nat Immunol* 6: 390–395, 2005.
49. Schmitz-Peiffer C, Browne CL, Oakes ND, Watkinson A, Chisholm DJ, Kraegen EW, Biden TJ. Alterations in the expression and cellular localization of protein kinase C isozymes epsilon and theta are associated with insulin resistance in skeletal muscle of the high-fat-fed rat. *Diabetes* 46: 169–178, 1997.
50. Schmitz-Peiffer C, Craig DL, Biden TJ. Ceramide generation is sufficient to account for the inhibition of the insulin-stimulated PKB pathway in C2C12 skeletal muscle cells pretreated with palmitate. *J Biol Chem* 274: 24202–24210, 1999.
51. Senn JJ. Toll-like receptor-2 is essential for the development of palmitate-induced insulin resistance in myotubes. *J Biol Chem* 281: 26865–26875, 2006.
52. Testa M, Rocca B, Spath L, Ranelletti FO, Petrucci G, Ciabattini G, Naro F, Schiaffino S, Volpe M, Reggiani C. Expression and activity of cyclooxygenase isoforms in skeletal muscles and myocardium of humans and rodents. *J Appl Physiol* 103: 1412–1418, 2007.
53. Weigert C, Brodbeck K, Staiger H, Kausch C, Machicao F, Haring HU, Schleicher ED. Palmitate, but not unsaturated fatty acids, induces the expression of interleukin-6 in human myotubes through proteasome-dependent activation of nuclear factor-kappaB. *J Biol Chem* 279: 23942–23952, 2004.
54. Wellen KE, Hotamisligil GS. Inflammation, stress, and diabetes. *J Clin Invest* 115: 1111–1119, 2005.
55. Yang M, Wu J, Martin CM, Kvietys PR, Rui T. Important role of p38 MAP kinase/NF-κB signaling pathway in the sepsis-induced conversion of cardiac myocytes to a proinflammatory phenotype. *Am J Physiol Heart Circ Physiol* 294: H994–H1001, 2008.



ELSEVIER



## The anti-apoptotic role of the unfolded protein response in Bcr-Abl-positive leukemia cells

Atsuko Tanimura<sup>a</sup>, Toshiaki Yujiri<sup>a,\*</sup>, Yoshinori Tanaka<sup>a</sup>, Masayuki Hatanaka<sup>a</sup>, Noriyuki Mitani<sup>a</sup>, Yukinori Nakamura<sup>a</sup>, Kazutoshi Mori<sup>b</sup>, Yukio Tanizawa<sup>a</sup>

<sup>a</sup> Department of Bio-Signal Analysis, Yamaguchi University Graduate School of Medicine, Ube, Yamaguchi 755-8505, Japan

<sup>b</sup> Department of Biophysics, Graduate School of Science, Kyoto University, Kyoto, Japan

### ARTICLE INFO

#### Article history:

Received 29 May 2008

Received in revised form 17 December 2008

Accepted 24 January 2009

Available online 23 February 2009

#### Keywords:

Unfolded protein response

Bcr-Abl

Apoptosis

### ABSTRACT

To define the role of the unfolded protein response (UPR) in leukemogenesis, we investigated UPR activation in the cells expressing the representative oncogene Bcr-Abl (B-A). The expression of UPR-related proteins and mRNAs, namely, X-box-binding protein (XBP1) and glucose-regulated protein 78 (GRP78) was increased in B-A. UPR inhibition using inositol-requiring enzyme 1 $\alpha$  (IRE1 $\alpha$ ) or activating transcription factor 6 (ATF6) dominant-negative mutants diminished the ability of Bcr-Abl to protect the cells from etoposide- and imatinib-induced apoptosis. We also noted that the expression of UPR-related genes in primary leukemia cells from Philadelphia chromosome (Ph)-positive cells was higher than that in the control by quantitative RT-PCR assay. Thus, our results suggested that UPR is a downstream target of Bcr-Abl and plays an anti-apoptotic role in Ph-positive leukemia cells.

© 2009 Elsevier Ltd. All rights reserved.

### 1. Introduction

The Bcr-Abl fusion protein plays a central role in chronic myeloid leukemia (CML) and Philadelphia chromosome (Ph)-positive acute leukemia. The molecular mechanism of leukemogenesis by Bcr-Abl has been the focus of intensive research over several decades. The transformation of hematopoietic cells by Bcr-Abl involves the assembly of multiprotein complexes and phosphorylation of several substrates, leading to the activation of signal transduction pathways that generate proliferative and anti-apoptotic signals.

The accumulation of unfolded proteins in the lumen of the endoplasmic reticulum (ER) induces a coordinated adaptive program termed as the unfolded protein response (UPR). The UPR alleviates stress by upregulating protein folding in the ER and inhibiting protein synthesis. In mammalian cells, the UPR is initiated by diverse signaling pathways whenever protein folding in the ER is compromised. Physiological conditions that induce the UPR by causing protein misfolding include the differentiation and development of professional secretory cells such as plasma cells or pancreatic  $\beta$  cells; altered metabolic conditions such as glucose deprivation and ischemia; mutations in the genes encoding secretory or transmembrane proteins, which are normally folded in the ER, such as insulin; and infection by certain pathogens, such as hepatitis C.

Although a number of studies have reported UPR activation in a variety of solid tumors, the UPR in cancers remains poorly characterized. It is not known whether UPR activation in cancers is solely due to microenvironmental stress or other mechanisms [1]. Moreover, the influence of the UPR on leukemogenesis remains largely uninvestigated. Here, we showed the constitutive activation of UPR in Bcr-Abl-expressing cells and demonstrated that the UPR plays a role in the anti-apoptotic effect of Bcr-Abl.

### 2. Materials and methods

#### 2.1. Cell culture

32Dcl3 mouse myeloid cells (RIKEN Cell Bank, Saitama, Japan) were cultured in RPMI 1640 medium supplemented with 10% FBS and 1 ng/ml recombinant murine IL-3. The vectors pZeo-p210 Bcr-Abl (B-A), pZeo-c-Abl (Abl), and pZeoSV2 (Mock) (Invitrogen, Carlsbad, CA, USA) were stably transfected into the 32Dcl3 cells using Nucleofector (Amaxa, Inc., Gaithersburg, MD, USA). The complementary DNAs encoding p210 Bcr-Abl and c-Abl were of human origin. Bcr-Abl-expressing cells were selected and cultured following IL-3 withdrawal. Abl and Mock were selected using 600  $\mu$ g/ml Zeocin and maintained with 350  $\mu$ g/ml Zeocin (Invitrogen). The expression plasmid for IRE1 $\alpha$  lacking the sequence of kinase and ribonuclease domain (IRE1 DN) [2] or for ATF6 $\alpha$  lacking the sequence of activation domain (amino acids 171–373) (ATF6 DN) [3] was stably transfected into B-A and Mock. Stable B-A or Mock transformants were selected using 300  $\mu$ g/ml or 1.2 mg/ml geneticin (Invitrogen), respectively. The stably transfected cells were used as cloned pools for the experiments in order to avoid the effects of clonal selection.

#### 2.2. Patients

This study was approved by the Institutional Review Board, and informed consent was obtained from all the patients and healthy controls. Samples obtained

\* Corresponding author. Tel.: +81 836 222251; fax: +81 836 222342.

E-mail address: [yujirit@yamaguchi-u.ac.jp](mailto:yujirit@yamaguchi-u.ac.jp) (T. Yujiri).

from 8 Ph-positive acute lymphoblastic leukemia patients (4, bone marrow (BM); 4, peripheral blood (PB)) and 12 healthy controls (7, BM; 5, PB) were analyzed. Mononuclear cells were collected using Lymphoprep (Axis-Shield, Oslo, Norway).

### 2.3. Immunoblot analysis

The following antibodies were used for immunoblot analysis; anti-Crk-L (sc-319) and anti-XBP1 (sc-7160) (Santa Cruz Biotechnology, Santa Cruz, CA, USA), anti-phospho-eIF2 $\alpha$  (Ser51) and anti-eIF2 $\alpha$  (Cell Signaling Technology, Inc., Beverly, MA, USA), anti-KDEL (SPA-827) (Stressgen, Ann Arbor, MI, USA), anti-c-Abl (OP20) (Calbiochem, San Diego, CA, USA), anti-GAPDH (MAB374) (Chemicon International, Inc., Temecula, CA, USA), and anti-Nucleoporin p62 (BD Biosciences, San Jose, CA, USA).

### 2.4. Luciferase assay

HEK293T cells with the ER stress response element (ERSE) or unfolded protein response element (UPRE) reporter [4] were transiently cotransfected with pZeo-p210 Bcr-Abl, pZeo-c-Abl, or an empty vector alone and the  $\beta$ -galactosidase expression plasmid pZeoSV2/lacZ using FuGENE6 (Roche Diagnostics, Indianapolis, IN, USA). After 48 h of incubation, luciferase activity was measured using the PicaGene reagent kit (Toyo Inki, Tokyo, Japan) according to the manufacturer's instructions and normalized to the corresponding  $\beta$ -galactosidase activity levels. 32Dcl3 cells stably expressing Bcr-Abl (B-A) or the empty vector (Mock) were analyzed by a luciferase assay using the ERSE or UPRE reporter with the pGL4.74 vector (Promega, Madison, WI, USA) as a normalized control.

### 2.5. Quantitative reverse transcription-polymerase chain reaction assay (RT-PCR) assay

Total RNA from the mononuclear cells was extracted using ISOGEN (Nippon Gene Co. Ltd., Tokyo, Japan) according to the manufacturer's instructions. Total RNA was subjected to reverse transcription with Superscript II Reverse Transcriptase (Invitrogen) according to the manufacturer's instructions. Quantitative RT-PCR assay of the indicated genes was performed using a QuantiTect SYBR Green PCR kit (Qiagen, Hilden, Germany) with a LightCycler system (Roche Diagnostics). The primer sequences for each of the murine UPR-related genes are as follows: spliced form of XBP1, 5'-gctgagtcgacgagcagggtgc-3' and 5'-catgacagggtccaactgtccag-3'; GRP78, 5'-gacattgccccagaagaaa-3' and 5'-ctcatgacattcagtcagca-3'; CHOP, 5'-cctagcttgctgacagag-3' and 5'-ctgctctctctctctatgc-3'; P58IPK, 5'-ccttatcgagacgtcttcg-3' and 5'-tcagagtcctgattcattcca-3'; ERdj4, 5'-cttagtggtgccaagtctgcc-3' and 5'-ccgagagtgttcattcagctcttg-3'; and GAPDH, 5'-ggcattgctctcaatgacaa-3' and 5'-atgtaggcatgaggtccac-3'. The primer sequences for each of the human UPR-related genes are as follows: spliced form of XBP1, 5'-tgagtcgacgagcagggtgc-3' and 5'-tggcaggctctggggaag-3'; GRP78, 5'-gagttcttcaatggcaagg-3' and 5'-ggggacatcatcaagcag-3'; EDEM, 5'-tctctctaccagcaacc-3' and 5'-cggtctctctggtgactgttc-3'; CHOP, 5'-cctatgttccctctctg-3' and 5'-tgacctctctggttctg-3'; and  $\beta$ -actin, 5'-caagagatggccacggctgct-3' and 5'-tcctctctcatctctgctgca-3'.

The calculated concentration was normalized to the expression level of  $\beta$ -actin or GAPDH mRNA.

### 2.6. Apoptosis assay

The cells were treated with 20  $\mu$ M etoposide or 1.5  $\mu$ M imatinib and incubated for 14 or 16 h, respectively. To measure the extent of apoptosis, the cells were stained using an Annexin-V-FLUOS staining kit (Roche Diagnostics). Cytomics FC500 (Beckman Coulter Inc., Fullerton, CA, USA) was used for flow cytometric analysis.

## 3. Results and discussion

To determine whether the Bcr-Abl oncoprotein altered the UPR, we evaluated the expression of UPR-related proteins. Bcr-Abl, c-Abl, or an empty vector was stably transfected into 32Dcl3 cells. Bcr-Abl-expressing cells (B-A) showed an upward shift in CrkL, a tyrosine-phosphorylated substrate by Bcr-Abl tyrosine kinase (Fig. 1a). The expression of the UPR-related proteins, namely, glucose-regulated protein 78 (GRP78) and the phosphorylated  $\alpha$ -subunit of eukaryotic translation initiation factor 2 $\alpha$  (eIF2 $\alpha$ ), was elevated in B-A as compared to that in c-Abl-transfected (Abl) or empty vector-transfected (Mock) cells under basal conditions (Fig. 1a). To confirm UPR upregulation, the cells were treated with an ER stress activator, thapsigargin. All the cells showed elevated levels of GRP78 and phosphorylated eIF2 $\alpha$  after treatment with thapsigargin. The upregulated expression of UPR-related proteins was consistently observed in B-A as compared to Mock and Abl (Fig. 1a). Treatment of the cells with another ER stress activator, tunicamycin produced the same result (data not shown). GRP78

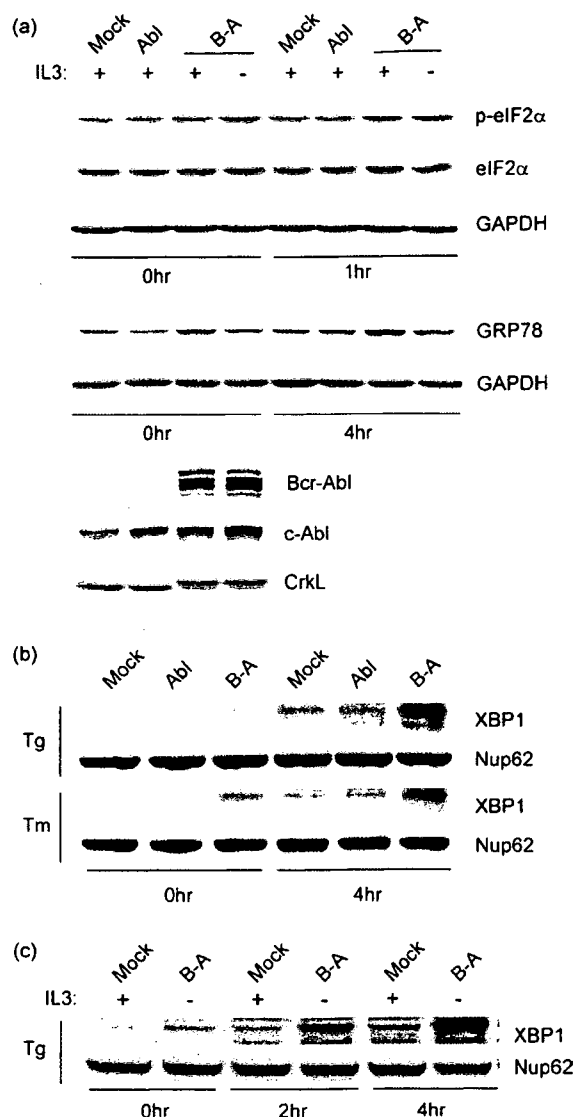


**Fig. 1.** The expression of UPR-related proteins is upregulated in Bcr-Abl-expressing cells. (a) B-A, Abl, and Mock were produced by transfecting 32Dcl3 cells with the vectors pZeo-p210 Bcr-Abl, pZeo-c-Abl, and pZeoSV2, respectively. The cells were treated with 600 nM thapsigargin for the indicated time periods. Immunoblot analysis was performed with the following antibodies; anti-CrkL, anti-eIF2 $\alpha$ , anti-phospho-eIF2 $\alpha$  (Ser51), anti-KDEL, anti-c-Abl, and anti-GAPDH. (b) XBP1 expression in nuclear lysates was analyzed using anti-XBP1 antibody. The cells were treated with either 600 nM thapsigargin (Tg) or 2  $\mu$ g/ml tunicamycin (Tm) for 4 h. Nucleoporin p62 was used as the loading control. All the cells were cultured in the presence of IL-3. (c) XBP1 expression in nuclear lysates was examined. The cells were treated with 600 nM thapsigargin for the indicated time periods.

is a key regulator of the UPR. As a Ca<sup>2+</sup>-binding molecular chaperone in the ER, GRP78 maintains ER homeostasis, suppresses stress-induced apoptosis, and controls UPR signaling. The phosphorylation of eIF2 $\alpha$  at Ser51 is an early event associated with the downregulation of protein synthesis at the level of translation and initiation of a transcriptional program. This constitutes a potent mechanism to overcome various stress conditions including ER stress. Furthermore, B-A in the presence or absence of IL-3 showed higher levels of the X-box-binding protein 1 (XBP1) in the nuclear extract than Abl or Mock did (Fig. 1b and c). The treatment with thapsigargin or tunicamycin clarified that nuclear XBP1 was increased by drug-induced ER stress and was consistently elevated in B-A as compared to that in Mock or Abl either in the presence or absence of IL-3 (Fig. 1b and c). XBP1 pre-messenger RNA is

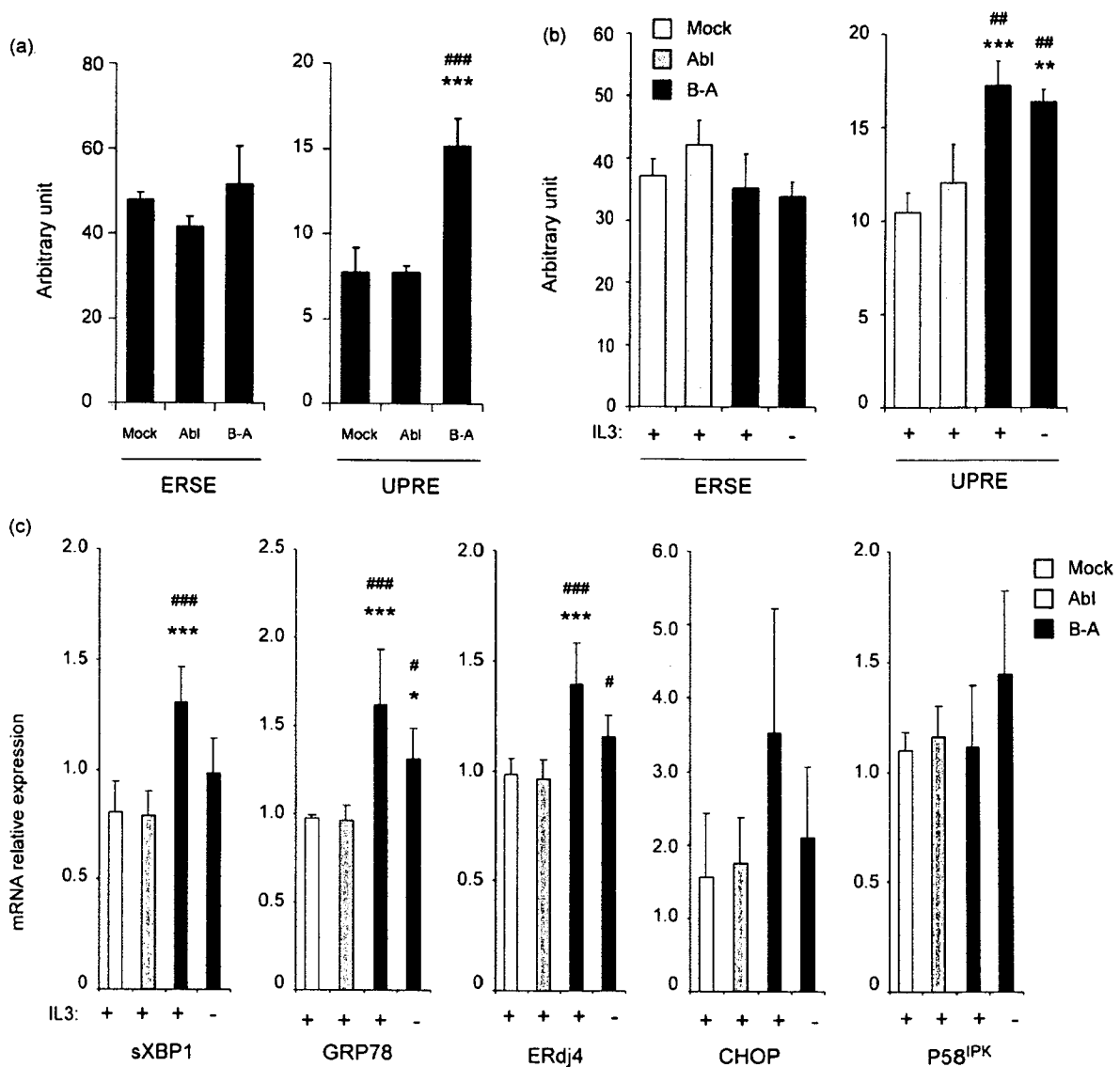


**Fig. 2.** Bcr-Abl enhances the expression of UPR-related mRNAs. (a) HEK293T cells with the ERSE or UPRE reporter were transiently cotransfected with the vectors pZeo-p210 Bcr-Abl (B-A), pZeo-c-Abl (Abl), or an empty vector alone (Mock) and the  $\beta$ -galactosidase expression plasmid pZeoSV2/lacZ. The data were statistically analyzed by one-factor ANOVA, followed by Fisher's PLSD test. The means  $\pm$  S.D. of 3 independent experiments are shown. (b) 32Dcl3 cells stably expressing Bcr-Abl (B-A), c-Abl (Abl) or an empty vector (Mock) were analyzed by a luciferase assay using the ERSE or UPRE reporter. Statistical analyses were performed using one-factor ANOVA followed by Fisher's PLSD test. The means  $\pm$  S.D. of 3 independent experiments are shown. (c) 32Dcl3 cells stably expressing Bcr-Abl (B-A), c-Abl (Abl), and an empty vector (Mock) were analyzed by a quantitative RT-PCR assay of the indicated genes. Statistical analyses were performed using one-factor ANOVA followed by Fisher's PLSD test. The means  $\pm$  S.D. of 4 independent experiments are shown. \* $P < 0.05$ , \*\* $P < 0.005$ , \*\*\* $P < 0.0005$ , compared to Mock. # $P < 0.05$ , ## $P < 0.005$ , ### $P < 0.0005$ , compared to Abl.

converted to mature mRNA by unconventional splicing that is mediated by the endonuclease inositol-requiring enzyme 1 (IRE1). The transcription factor protein XBP1 spliced, which is translated from mature XBP1 mRNAs, contains a nuclear localization signal and a transcriptional activation domain and activates the transcription of target genes in the nucleus.

To examine whether Bcr-Abl induces the UPR-related transcriptional activity, we performed the luciferase reporter assay. Bcr-Abl, c-Abl, or an empty vector was transiently transfected into HEK293T cells with the ERSE or UPRE reporter construct [4]. ERSE-mediated transcriptional activity did not considerably differ between Mock, Abl, and B-A. In addition, the nuclear levels of activating transcription factor 6 (ATF6), an ERSE-binding transcription factor, also did not significantly differ between Mock, Abl, and B-A (data not shown). On the other hand, UPRE-mediated transactivation in B-A was significantly increased as compared to that in Mock or Abl (Fig. 2a). Similar results were obtained in the 32Dcl3 cells stably

expressing Bcr-Abl in the presence or absence of IL-3 (Fig. 2b). These data suggested that Bcr-Abl-induced UPR was regulated, at least, through UPRE-mediated transcriptional activation. Next, we investigated the expression of UPR-related genes in Bcr-Abl-expressing 32Dcl3 cells. The mRNA expression of the spliced form of XBP1; GRP78; C/EBP-homologous protein-10 (CHOP); ERdj4, a mammalian chaperone that belongs to the HSP40 protein family; and the cochaperone protein p58<sup>IPK</sup> was analyzed using a quantitative RT-PCR assay. GAPDH mRNA expression was used as a normalized control. The mRNA expression of the spliced form of XBP1, GRP78, and ERdj4 was significantly increased in B-A. Meanwhile, the mRNA expression of CHOP and p58<sup>IPK</sup> showed no significant increase in B-A (Fig. 2c). Taken together, our data suggested that Bcr-Abl constitutively induced the UPR, which subsequently increased the expression of several UPR-related mRNAs.

We intended to understand the contribution of the UPR to Bcr-Abl-induced leukemogenesis. To define the role of the UPR in

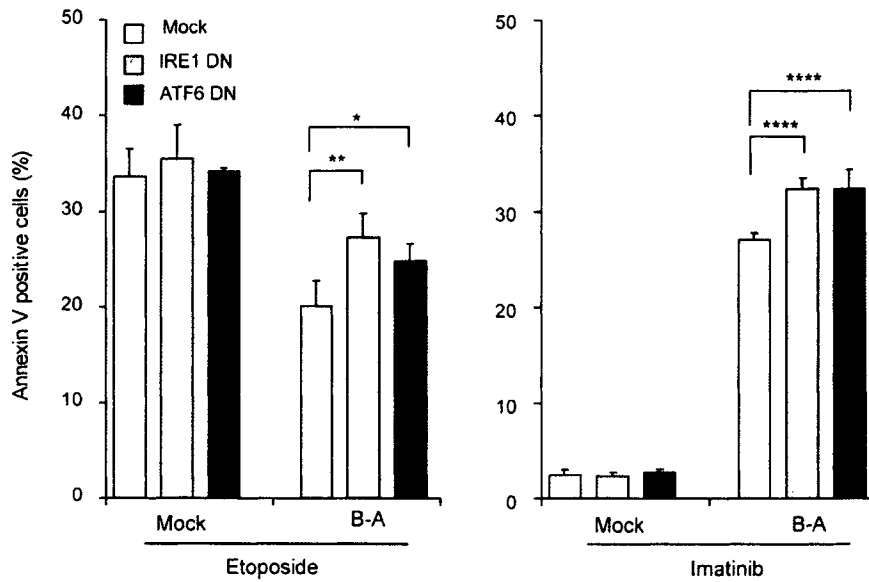


**Fig. 3.** Dominant-negative mutants of IRE1 $\alpha$  and ATF6 reduce the anti-apoptotic effects of Bcr-Abl. The expression plasmid for IRE1 $\alpha$  lacking the sequence of the kinase and ribonuclease domains (IRE1 DN) or that for ATF6 $\alpha$  lacking the sequence of the activation domain (amino acids 171–373) (ATF6 DN) was stably transfected into cells expressing Bcr-Abl (B-A) and an empty vector (Mock). Apoptosis assay was independently repeated 3 times. The means  $\pm$  S.D. of 3 independent experiments are shown. Statistical analyses were performed using one-factor ANOVA followed by Fisher's PLSD test. \* $P < 0.05$ ; \*\* $P < 0.01$ ; \*\*\*\* $P < 0.0001$ .

Bcr-Abl-expressing cells, the dominant-negative mutants of ATF6 [3] or IRE1 $\alpha$  [2] were stably transfected into Mock and B-A. The expression of the dominant-negative ATF6 (ATF6 DN) or IRE1 $\alpha$  (IRE1 $\alpha$  DN) did not affect the proliferation rate of either Mock or B-A in the presence or absence of IL-3 (data not shown). Thus, the ATF6- or IRE1 $\alpha$ -mediated UPR did not exert any effect on Bcr-Abl-induced proliferation or IL-3 dependency. On the other hand, the number of apoptotic cells induced by the genotoxin

etoposide was significantly increased in both ATF6 DN- and IRE1 $\alpha$  DN-transfected B-A than in empty vector-transfected B-A. Interestingly, treatment with imatinib, a specific Abl tyrosine kinase inhibitor, also resulted in a greater number of apoptotic cells in mutant-transfected B-A than in the control (Fig. 3). Thus, these data suggested that the ATF6- or IRE1 $\alpha$ -UPR signaling pathways were associated with the anti-apoptotic effect of the Bcr-Abl oncoprotein. The data obtained from the ATF6 mutant suggested that ATF6

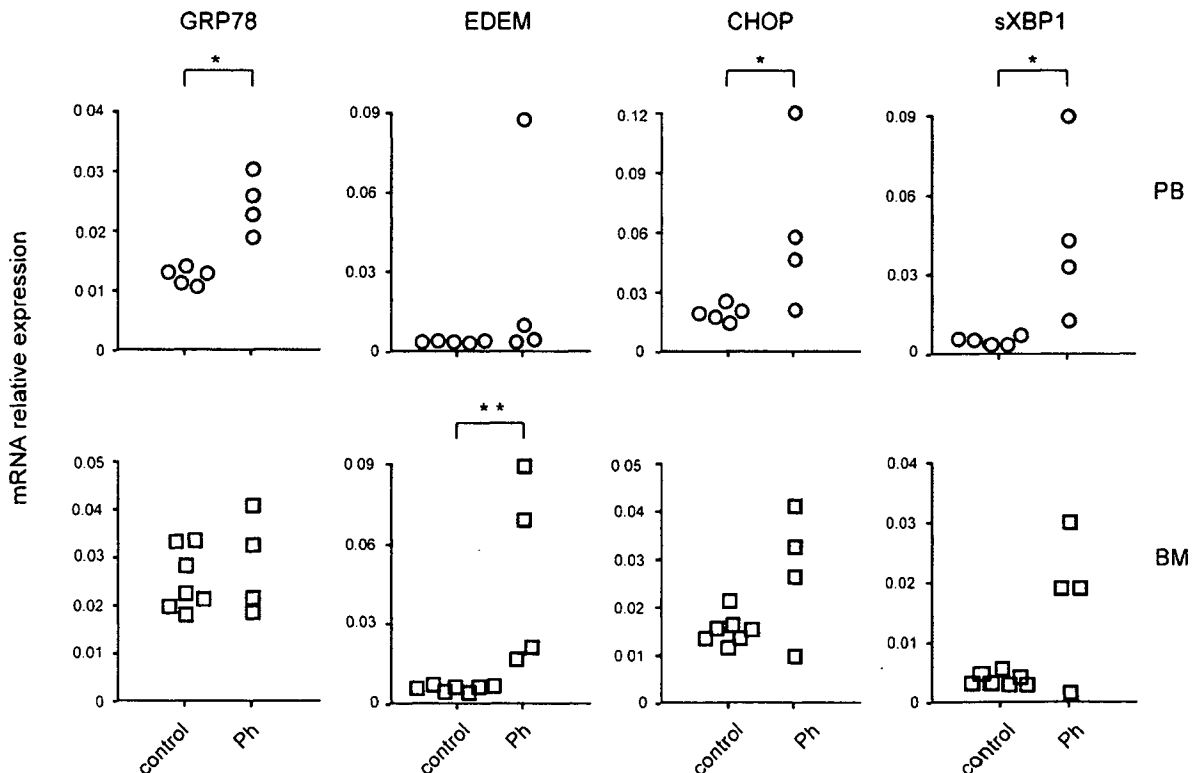


**Fig. 4.** The levels of UPR-related mRNAs are increased in Ph-positive primary acute leukemia cells. The data were statistically analyzed by Mann–Whitney *U*-test. \* $P < 0.05$ ; \*\* $P < 0.01$ .



was a transcription factor that contributed to the Bcr-Abl-induced cell survival of cells following anticancer drug administration, even though the levels of the nuclear ATF6 protein and ERSE-mediated transactivation were not increased by Bcr-Abl. Recently, ATF6 $\alpha$  was reported to heterodimerize with XBP1 for the induction of ER-associated degradation components, a part of the UPR [5]. ATF6 mutant might inhibit the ATF6-XBP1 heterodimerization and eventually decrease UPR-mediated transactivation. IRE1 $\alpha$  mutants lacking the cytosolic effector domain inhibit the activation of XBP1 by inhibiting the ribonuclease activity. Further, they inhibit the autophosphorylation of IRE1 $\alpha$ , which in turn induces the formation of the complex of tumor necrosis factor receptor associated factor 2 (TRAF2), apoptosis signal-regulating kinase 1 (ASK1) [6], and Bax/Bak, proapoptotic Bcl-2 family proteins [7]. IRE1 $\alpha$  might regulate the Bcr-Abl-induced survival pathway via XBP1 activation, modification of IRE1 $\alpha$ -TRAF2-ASK1 signaling, and the IRE1 $\alpha$ -Bax-Bak complex formation. Further studies are required to elucidate the mechanisms of Bcr-Abl-IRE1 $\alpha$  signaling. Our data also showed that the phosphorylation of eIF2 $\alpha$  was constitutively elevated in B-A (Fig. 1). However, the mechanism of eIF2 $\alpha$  activation by Bcr-Abl remains to be elucidated. Since the UPR has both protective and destructive roles, it is essential to fully characterize the branches and downstream components of the UPR that are activated in Bcr-Abl-expressing cells.

Finally, we investigated whether primary Ph-positive acute leukemia cells showed UPR activation. We analyzed the mRNA expression of UPR-related genes, namely, GRP78, ER-degradation enhancing  $\alpha$ -mannosidase-like protein (EDEM), CHOP, and the spliced form of XBP1, in Ph-positive acute lymphoblastic leukemia cells by real-time RT-PCR analysis. Most of the PB or BM mononuclear cells analyzed were Ph-positive leukemia cells. The mRNA expression of GRP78, CHOP, and the spliced form of XBP1 was significantly increased in the PB leukemia cells and that of EDEM was significantly increased in the BM leukemia cells (Fig. 4). The mRNA expression levels of CHOP and the spliced form of XBP1 in the BM of patients tended to be higher than those in the control BM mononuclear cells. These data suggested that the UPR is activated in primary Ph-positive acute leukemia cells. Although these leukemia cells may express p190 Bcr-Abl in contrast to p210 Bcr-Abl in the transformed 32Dcl3 cells, these Bcr-Abl subtypes appear to function in a similar manner in the induction of UPR.

In this study, we showed that Bcr-Abl-expressing cells exhibit an increased UPR. This increased response plays a significant anti-apoptotic role. There is increasing evidence that the UPR is activated in a variety of solid tumors, from patients and in animal models such as breast cell tumors, hepatocellular carcinomas, and gastric tumors [1]. The mechanism underlying the balance between cell-survival and cell-death signals initiated by UPR activation in cancers is unclear. The UPR serves to protect the cells from normal variations occurring in the cellular environment, which arise from changes in the blood nutrient levels and increase in toxic substances. A range of pathological conditions can also activate the UPR. Tumor cells encounter deficiency of oxygen and nutrients. Under such circumstances, the UPR can be induced in these cells. Furthermore, tumor cells produce several survival factors such as autocrine or paracrine stimulators, invasion and metastatic regulators such as matrix met-

alloproteinases, and transmembrane proteins such as adhesion molecules to initiate survival formation around the microenvironments. Several studies have indicated that UPR activation probably plays a crucial role in tumor growth. It has been demonstrated using XBP1-deficient cells and XBP1-knockdown cells that XBP1 is required for tumor growth in vivo [8]. The XBP1-induced UPR has also been shown to play a key role in the pathogenesis of plasma cell myeloma [9]. Our preliminary observation indicated that UPR was also upregulated in some primary Ph-negative leukemia cells (data not shown). Therefore, the activation of the UPR might be a common mechanism in both solid tumor and leukemia cells. We showed that the suppression of the UPR enhanced the anti-leukemic effects of imatinib and etoposide in Bcr-Abl-expressing cells. In Ph-positive leukemia cells, the apoptosis-inducing mechanism of imatinib was considerably different from that of etoposide. Therefore, targeting the UPR may provide useful alternative approaches for the treatment of Ph-positive leukemia such as an imatinib resistant-CML clone or Ph-positive acute leukemia.

#### Conflict of interest statement

The authors declare no competing financial interests.

#### Acknowledgements

This work was supported by Grants-in-Aid from the Ministry of Education, Culture, Sports, Science and Technology, Japan; UBE Kosan Foundation; and Yamaguchi University Foundation.

**Contributions:** All authors contributed to this paper; in particular, A.T., T.Y., Y.T., M.H., N.M., and Y.N. contributed to experimental work. T.Y. wrote the manuscript. K.M. and Y.T. contributed to the proofreading of the manuscript.

#### References

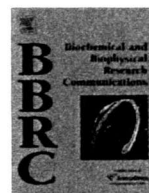
- [1] Ma Y, Hendershot LM. The role of the unfolded protein response in tumour development: friend or foe? *Nat Rev Cancer* 2004;4:966–77.
- [2] Miyoshi K, Katayama T, Imaizumi K, Taniguchi M, Mori Y, Hitomi J, et al. Characterization of mouse Ire1 alpha: cloning, mRNA localization in the brain and functional analysis in a neural cell line. *Brain Res Mol: Brain Res* 2000;85:68–76.
- [3] Yoshida H, Okada T, Haze K, Yanagi H, Yura T, Negishi M, et al. ATF6 activated by proteolysis binds in the presence of NF- $\kappa$ B (CBF) directly to the cis-acting element responsible for the mammalian unfolded protein response. *Mol Cell Biol* 2000;20:6755–67.
- [4] Yoshida H, Matsui T, Hosokawa N, Kaufman RJ, Nagata K, Mori K. A time-dependent phase shift in the mammalian unfolded protein response. *Dev Cell* 2003;4:265–71.
- [5] Yamamoto K, Sato T, Matsui T, Sato M, Okada T, Yoshida H, et al. Transcriptional induction of mammalian ER quality control proteins is mediated by single or combined action of ATF6 $\alpha$  and XBP1. *Dev Cell* 2007;13:365–76.
- [6] Urano F, Wang X, Bertolotti A, Zhang Y, Chung P, Harding HP, et al. Coupling of stress in the ER to activation of JNK protein kinases by transmembrane protein kinase IRE1. *Science* 2000;287:664–6.
- [7] Hetz C, Bernasconi P, Fisher J, Lee AH, Bassik MC, Antonsson B, et al. Proapoptotic BAX and BAK modulate the unfolded protein response by a direct interaction with IRE1 $\alpha$ . *Science* 2006;312:572–6.
- [8] Romero-Ramirez L, Cao H, Nelson D, Hammond E, Lee AH, Yoshida H, et al. XBP1 is essential for survival under hypoxic conditions and is required for tumor growth. *Cancer Res* 2004;64:5943–7.
- [9] Carrasco DR, Sukhdeo K, Protopopova M, Sinha R, Enos M, Carrasco DE, et al. The differentiation and stress response factor XBP-1 drives multiple myeloma pathogenesis. *Cancer Cell* 2007;11:349–60.



ELSEVIER

Contents lists available at ScienceDirect

# Biochemical and Biophysical Research Communications

journal homepage: [www.elsevier.com/locate/ybbrc](http://www.elsevier.com/locate/ybbrc)

## DOC2b is a SNARE regulator of glucose-stimulated delayed insulin secretion

Mutsuko Miyazaki, Masahiro Emoto\*, Naofumi Fukuda, Masayuki Hatanaka, Akihiko Taguchi, Sachiko Miyamoto, Yukio Tanizawa

Division of Endocrinology, Metabolism, Hematological Sciences and Therapeutics, Department of Bio-Signal Analysis, Yamaguchi University Graduate School of Medicine, 1-1-1 Minami-Kogushi, Ube 755-8505, Japan

### ARTICLE INFO

#### Article history:

Received 23 April 2009

Available online 3 May 2009

#### Keywords:

Biphasic insulin secretion

DOC2b

Calcium

SNARE

Syntaxin4

Vesicular trafficking

### ABSTRACT

Insulin secretion is precisely regulated by blood glucose with unique biphasic pattern. The regulatory mechanism of the second-phase insulin release is unclear. In this study, we report that DOC2b (double C2 domain protein isoform b), a SNARE related protein, was associated with insulin vesicles and translocated to plasma membrane within several minutes upon high-glucose stimulation followed by an interaction with syntaxin4, but not syntaxin1. This binding specificity and the time course of DOC2b translocation were suitable for the regulation of second-phase insulin release. Increased DOC2b expression enhanced glucose-stimulated insulin secretion. In contrast, silencing DOC2b inhibited delayed release of insulin, without affecting rapid (~7 min) phase secretion. Interestingly, DOC2b had no effects on KCl-triggered insulin release. These data suggest that DOC2b may be a regulator for delayed (second-phase) insulin secretion in MIN6 cells.

© 2009 Elsevier Inc. All rights reserved.

### Introduction

Appropriate secretion of insulin from pancreatic  $\beta$ -cells is critically important to the energy homeostasis. The secretion of this hormone is precisely regulated by blood glucose with unique biphasic pattern [1,2]. The first-phase occurs just after exposure to glucose, followed by prolonged second-phase release. Fundamental mechanisms of glucose-stimulated first-phase release have been vigorously studied for a few decades. It involves the following sequential steps: rise in the ATP/ADP ratio by oxidative glycolysis, closure of ATP-sensitive potassium ( $K_{ATP}$ ) channels, depolarization of the plasma membrane, opening of voltage-dependent calcium channels, increase in intracellular calcium concentration ( $[Ca^{2+}]_i$ ), and activation of membrane fusion machinery [3–5]. Whereas, the second-phase of glucose-induced insulin secretion is regulated mainly by  $K_{ATP}$  channel-independent pathway [6,7]. Despite intensive investigations, however, the mechanisms of second-phase release are still largely unknown.

In the view of insulin granule dynamics in  $\beta$ -cells, insulin secretion is primarily achieved by membrane fusion processes of insulin granules to plasma membrane. These processes are mediated by a set of highly conserved membrane proteins known as SNARE machinery (i.e. syntaxins, VAMPs, SNAPs), and its regulatory proteins [8–16]. However, little is known about the precise mechanisms how glucose regulates SNARE machinery. Notably, no SNARE regulator has been identified for the second-phase of insulin

exocytosis. In neurons, calcium sensor proteins such as synaptotagmins have critical roles in vesicle fusion process through the binding to SNARE proteins [17,18]. Although some isoforms of synaptotagmins have been identified in pancreatic  $\beta$ -cell [19–21], there are no definite evidences that synaptotagmins regulate insulin secretion to date.

The universal role of  $Ca^{2+}$  as a trigger for regulated exocytosis predicts the existence of conserved proteins capable of activating the fusion machinery upon binding  $Ca^{2+}$  in pancreatic  $\beta$ -cells. Although many proteins have been suggested to play such a role in many type of cells, tandem C2 domain proteins have attracted the most attentions as the putative calcium sensors. DOC2 (double C2 domain) protein family have identified as a novel protein having tandem C2 domains that targeted to membrane phospholipids in  $[Ca^{2+}]_i$  dependent manner [22,23]. Many proteins have been identified to be involved in the insulin-vesicle fusion in pancreatic  $\beta$ -cells [19,20,24,25]; however, there are no candidates of  $Ca^{2+}$  sensor proteins suitable for relatively slow second-phase release. Furthermore, the connection between glucose and calcium signals in the second-phase insulin secretion is also obscure.

Previously, we have investigated the functional role of DOC2b (one of the isoforms of DOC2 family proteins) on exocytosis in adipocytes and found that it regulates the relatively slow-time scale (several minutes order) step of vesicle fusion [26,27]. Herein, we showed that DOC2b was translocated from intracellular compartment to the plasma membrane upon glucose stimulation, and bound syntaxin4, but not syntaxin1, in pancreatic  $\beta$ -cells. This binding was  $[Ca^{2+}]_i$  dependent. DOC2b expression enhanced and its silencing inhibited delayed insulin secretion. Our data

\* Corresponding author. Fax: +81 836 22 2342.

E-mail address: [emotom@yamaguchi-u.ac.jp](mailto:emotom@yamaguchi-u.ac.jp) (M. Emoto).

suggested that DOC2b may be a positive regulator of membrane fusion and have a role on second-phase secretion of insulin.

## Materials and methods

**Reagents and antibodies.** Mouse DOC2 cDNA constructs (DOC2a, DOC2b) were kindly provided by Dr. Rory Duncan (University of Edinburgh, UK). The polyclonal antibody against to DOC2a and DOC2b were generated against the peptide sequence CYLKELEQAEGPGL and CGARDDDEDVDQL, respectively. Monoclonal anti-myc antibody (Clone 9E10) was from Covance (NJ, USA). The other antibodies to DOC2b, syntaxin4, syntaxin1A were products of Synaptic Systems GmbH (Goettingen, Germany). The siRNA duplex and control oligonucleotides were synthesized by Invitrogen (CA, USA).

**Cell culture.** MIN6 cells (a gift from Dr. Jun-ichi Miyazaki, Osaka University [28]) were grown in Dulbecco's modified Eagle's medium (DMEM) containing 25 mM glucose supplemented with 15% fetal bovine serum, 100 U/ml penicillin, 100 µg/ml streptomycin and 5 µl/L β-mercaptoethanol at 37 °C in a humidified atmosphere (5% CO<sub>2</sub>). Cells were passaged every 4–5 days at 70–80% confluence. For retrovirus packaging, Plat-E cells were maintained in DMEM containing 10% fetal bovine serum, 1 µg/ml puromycin (Sigma, MO, USA), and 10 µg/ml blasticidin S (Funakoshi, Tokyo, Japan).

**RT-PCR.** Total RNA was extracted from MIN6 cells using ISOGEN (NIPPON GENE, Tokyo, Japan). Purified RNA was converted to cDNA by SuperScriptII reverse transcriptase (Invitrogen). RT-PCR was performed using the following primers: DOC2a forward; 5'-TCGCATGACCATCAACATCC-3', DOC2a reverse; 5'-CTTCAGGTAACAGGATATGC-3', DOC2b forward; 5'-AAAGGATCCAAGGCAGAGGACAAGTCTCTGG-3', DOC2b reverse; 5'-AAACTCGAGTCAGTCGCTACTACAGCCC-3'.

**Preparation of adenoviruses and transfection.** Adenovirus producing myc-tagged DOC2b and eGFP were prepared by AdEasy Adenoviral Vector System (Stratagene, CA, USA) according to the manufacturer's instructions. All amplified viruses were purified by the cesium chloride centrifugation method and stored at -80 °C. MIN6 cells were infected by these adenoviruses with the m.o.i. of ~30.

**Immunoprecipitation and immunoblotting.** Cells were lysed in lysis buffer [20 mM Hepes (pH 7.2), 100 mM NaCl, 1 mM EDTA, 25 mM NaF, 1 mM sodium vanadate, 1 mM benzamide, 5 µg/ml leupeptin, 5 µg/ml aprotinin, 1 mM phenylmethylsulfonyl fluoride, 1 mM DTT] and the protein concentration was measured with BCA protein assay reagent (Pierce, IL, USA). For immunoprecipitation, the cell lysate was preincubated with protein-G Sepharose at 4 °C for 1 h to remove nonspecific bindings. Then, samples were incubated with primary antibody at 4 °C for 8–12 h followed by incubation with protein-G Sepharose. Lysates and immunoprecipitates were resolved by SDS-PAGE and transferred to polyvinylidene difluoride membranes (GE Healthcare, UK). The membranes were incubated with primary antibodies for 8–12 h. Protein signals were visualized using horseradish peroxidase-conjugated secondary antibodies and enhanced chemiluminescence substrate kit (GE Healthcare, UK).

**DOC2b-shRNA construct, retrovirus preparation and generation of stable cell line.** Short hairpin-RNA was designed to have a 5'-AAGC-CAGATGTAGACAAGAAATC-3' sequence. Synthetic complementary single-stranded DNA of the target sequence was annealed, and the double-stranded DNA was inserted into RNAi-Ready pSIREN-RetroQ vector (Clontech, CA, USA). This plasmid vector was transfected into Plat-E to obtain the viruses using Lipofectamine 2000 transfection reagent (Invitrogen). Forty-eight hours after the transfection, supernatants containing retroviruses were harvested and purified by centrifugation and filtration. MIN6 cells were infected

with these retroviruses and kept in culture containing 1 µg/ml puromycin for at least 1 week to obtain stable cell-lines lacking DOC2b.

**Measurement of insulin secretion.** MIN6 cells were seeded and grown in 24-well plates for 3–4 days. The cells were preincubated in KRH buffer containing 3 mM glucose for 30 min at 37 °C. Then the cells were treated with 0, 3, 12 or 25 mM glucose with or without 30 mM KCl for 60 or 7 min. At the end of incubation, KRH buffer (supernatant) were stored for insulin determination. The cell was lysed in 0.5% NP-40 and used for the determination of protein concentration. Insulin concentrations were measured using Rat insulin ELISA kit (Morinaga, Yokohama, Japan). The results were normalized by cellular protein content.

**Immunofluorescence and immunoelectron microscopy.** Immunostaining and sample preparation for fluorescence and electron microscopy were performed by the methods described previously [27,29]. See detailed in Supplementary methods.

## Results

### Expression profile of DOC2 proteins in MIN6 cells and mouse islets

DOC2 family protein was identified as a group of type C tandem C2 domain proteins in neuron and was reported to regulate docking and fusion of synaptic vesicles in [Ca<sup>2+</sup>]<sub>i</sub> dependent manner [22,23]. This protein family consists of three isoforms, DOC2a, -b and -γ. DOC2a have been reported to be expressed in neuronal cells, whereas DOC2b is more widely expressed. DOC2γ is localized to the nucleus and has no Ca<sup>2+</sup>-binding activity because of amino acid substitutions at the Ca<sup>2+</sup> binding site [30]. Therefore, to clarify the involvement of DOC2 proteins in insulin secretion, we first investigated the presence of DOC2a and -b mRNA in the insulin-secreting cells MIN6. As shown in Fig. 1A, both DOC2 mRNAs were expressed in MIN6 cells. We next determined the protein expression of DOC2a and b in insulin-secreting cells by Western blotting. As shown in Fig. 1B, DOC2b isoform is predominantly expressed in pancreatic β-cells. Therefore, we focused on DOC2b protein as a candidate of Ca<sup>2+</sup> sensor for insulin secretion.

### DOC2b translocates to plasma membrane in response to glucose

Since DOC2b was reported to localized in the cytosol under the basal condition and translocated to plasma membrane upon stimulation in neuronal cells [31,32], we determine the subcellular localization of DOC2b in MIN6 cells. We performed immunofluorescent microscopy using polyclonal anti-DOC2b antibody or the cells expressing myc-tagged DOC2b. The confocal images showed that endogenous DOC2b, as well as expressed myc-DOC2b, was distributed throughout the cells in the basal state of 3 mM glucose. In contrast, when the cells were treated with high glucose (12 or 25 mM), DOC2b was translocated to the plasma membrane as shown in Fig. 2A. Interestingly, cell-permeable calcium chelating agent BAPTA-AM inhibited DOC2b translocation. Moreover, we

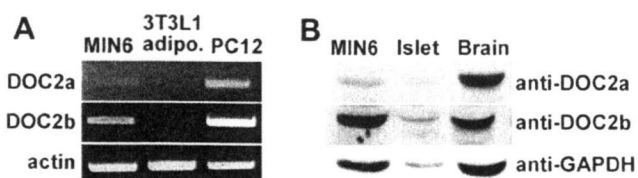


**Fig. 1.** Expression profiles and distributions of DOC2 proteins. (A) The expression of DOC2a and DOC2b in MIN6 cells, 3T3-L1 adipocytes, and PC12 were analyzed by RT-PCR. (B) Endogenous DOC2 proteins in MIN6 cells, mouse islet and mouse brain were determined by Western blot using anti-DOC2b and DOC2a antibodies.

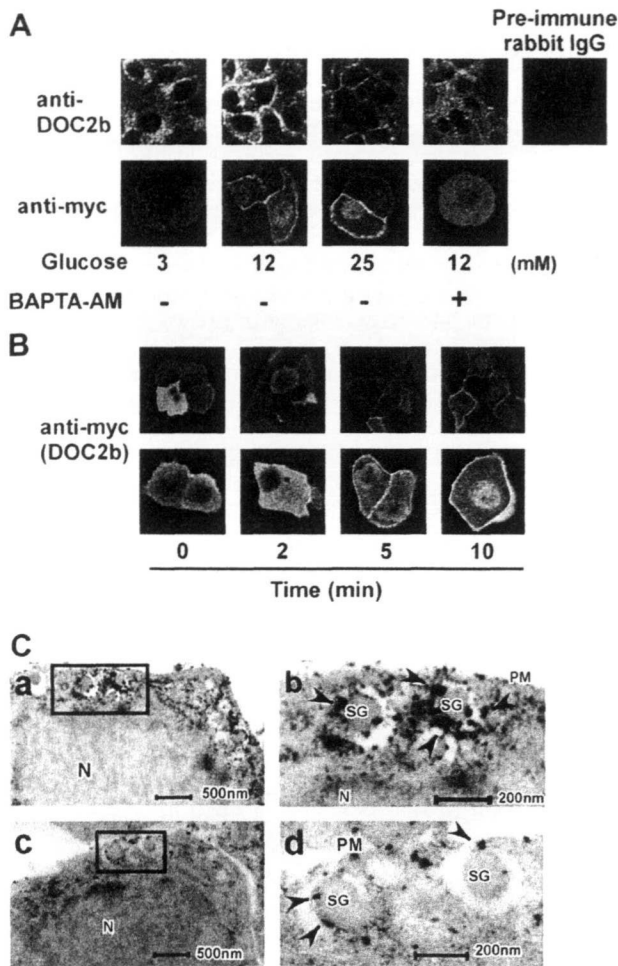


**Fig. 2.** Intracellular localization of DOC2b in MIN6 cells. (A,B) MIN6 cells were expressed or left untreated with adenovirus containing myc-tagged DOC2b 48 h prior to experiments. After the preincubation in KRH buffer for 0.5 h, cells were treated with 3, 12 or 25 mM glucose for 10 min (A) or the time indicated (B) and fixed followed by immunostaining with anti-DOC2b (for determination of endogenous expression) or anti-myc antibody followed by FITC-labeled secondary antibody. Stained cells were observed by confocal microscopy. In order to determine the role of  $[Ca^{2+}]_i$ , some cells were pre-treated with 30 mM BAPTA-AM for 30 min. The cells staining with normal rabbit IgG were used for negative control. C: Ultrathin-section of MIN6 cells were immunolabeled with anti-DOC2b antibody using avidin–biotin complex method and observed under a Hitachi H-7500 electron microscope without uranyl acetate or lead staining. Arrow heads show the staining detected by anti-DOC2b antibody. Panel b and d are enlarged images of a and c, respectively. SG, secretory granule; N, nucleus; PM, plasma membrane.

determined the time scale of DOC2b translocation in MIN6 cells. As shown in Fig. 2B, DOC2b was accumulated at plasma membrane about 5–10 min after the glucose stimulation. This relatively slow-time scale of DOC2b translocation is not suitable for the first-phase secretion of insulin.

#### DOC2b is localized at insulin vesicles

Since DOC2b has double C2 domains, it can be targeted to the membrane phosphatidyl inositols [33]. To confirm the precise membrane localization of endogenous DOC2b in pancreatic  $\beta$ -cells, we examined ultrathin-sections of MIN6 cells by immunoelectron microscopy using anti-DOC2b antibody. Interestingly, DOC2b-immunoreactive density was mostly found on the periphery of large dense core granules (insulin vesicles) near the plasma membrane (Fig. 2C).

#### DOC2b binds to syntaxin4 upon glucose stimulation

Recently we found a novel mechanism that DOC2b regulates membrane fusion through binding to syntaxin4 in adipocytes [27]. To investigate the role of DOC2b on insulin secretion, we first determined the DOC2b-binding partner in MIN6 cells. As shown in Fig. 3A and B, DOC2b–syntaxin4 binding was increased upon glucose stimulation and pre-treatment with BAPTA-AM decreased this interaction, suggesting that high glucose triggers DOC2b–syntaxin4 interaction in the presence of calcium ions. Since recent studies suggest that syntaxin1 was a t-SNARE for first-phase insulin secretion in pancreatic  $\beta$ -cells [12], we next assessed the interaction between DOC2b and syntaxin1 by immunoprecipitation experiments. As shown in Fig. 3A and C, DOC2b–syntaxin1 interaction was under the detectable level. These results, taken together with the data shown in Fig. 2, suggest the possibility that DOC2b regulates the second-phase insulin secretion through binding with syntaxin4.

#### DOC2b positively regulates glucose-stimulated insulin secretion

We next focused on the role of DOC2b in glucose-stimulated insulin secretion in MIN6 cells. As shown in Fig. 4A, adenoviral overexpression of myc-DOC2b in MIN6 cells caused significant increase in insulin secretion compared with control cells ( $p < 0.05$ ,  $n = 3$ ) at high glucose concentration. Next, we introduced short hairpin-RNA ( $shRNA_{DOC2b}$ ) into MIN6 cells by retroviral system to induce specific degradation of the DOC2b mRNA. Under these conditions, DOC2b protein expression was decreased to 10–20% of the control level (Fig. 4B). Using this stable cell-line lacking DOC2b, we measured rapid and prolonged (delayed) insulin secretion in response to glucose. As shown in Fig. 4C, insulin secretion for the first 60 min period was decreased by 20–54% in DOC2b silenced cells, compared with the control cells. However, during the first 7 min after glucose stimulation, we could not find any differences between the cells. These results raise the possibility that DOC2b may regulate second-phase secretion of insulin in MIN6 cells. In order to better assess this phase-dependency of DOC2b on insulin secretion, we conducted additional experiment using depolarization dependent, first-phase specific secretagogue KCl. As expected, KCl-stimulated insulin secretion did not differ both in DOC2b over-expressing and silencing cells compared to the respective control cells. These results support the aforementioned hypothesis that DOC2b may involve in the second-phase secretion of insulin.

#### Discussion

Insulin secretion is fundamentally important for glucose homeostasis and strictly regulated by blood glucose. However, its precise regulatory mechanism is not fully understood. In general, vesicular exocytosis occurs when appropriate stimulus (i.e. an increase in  $[Ca^{2+}]_i$ ) arrives to trigger the fusion of secretory vesicles with the plasma membrane. These membrane fusion processes are initiated with the formation of core complex consisting of SNARE proteins [18]. However, a number of additional factors are required to bring membrane fusion *in vivo*. These factors are called SNARE regulators. In pancreatic  $\beta$ -cells, a lot of SNARE regulators such as synaptotagmins I, II, III, V, and VII, were initially reported to be involved in insulin-granule exocytosis [19–21], but there remains uncertainty about their specificity [5]. Since we recently identified DOC2b as a positive SNARE regulator for the fusion step of vesicles containing glucose transporter 4 (GLUT4) in adipocytes [27], we speculatively investigated the role of DOC2b on insulin secretion in MIN6 cells.

In this report, we first confirmed the expression of DOC2b in islets and MIN6 cells (Fig. 1). Then, we revealed that DOC2b was localized around the insulin vesicles at cell periphery (Fig. 2C),

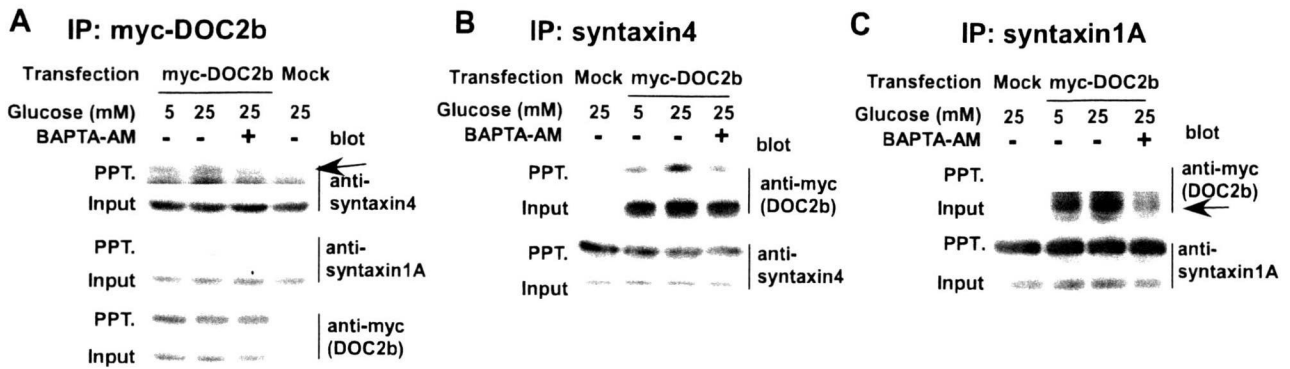


**Fig. 3.** DOC2b interacts with syntaxin4 in glucose and  $\text{Ca}^{2+}$  dependent manner. Myc-tagged DOC2b and eGFP control (Mock) were expressed in MIN6 cells by adenovirus vectors. After the preincubation for 30 min in KRH buffer containing 5 mM glucose, the cells were treated with 5 or 25 mM glucose for 15 min in the presence or absence of 30 mM BAPTA-AM. Immunoprecipitation was performed by monoclonal anti-myc (A), polyclonal anti-syntaxin4 (B), or monoclonal anti-syntaxin1A (C) antibodies. Precipitates were separated by SDS-PAGE and blotted with anti-myc, anti-syntaxin4, and anti-syntaxin1A antibodies.

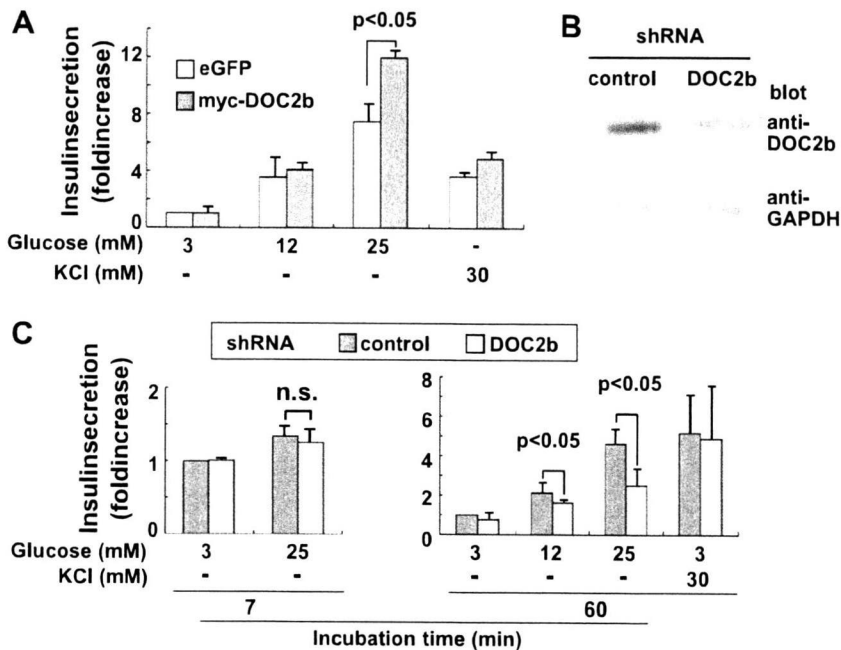


**Fig. 4.** Role of DOC2b on glucose-stimulated insulin secretion in MIN6 cells. MIN6 cells expressing DOC2b (A) or shRNA<sub>DOC2b</sub> (B,C) were treated with 3, 12, 25 mM glucose or 30 mM KCl for 60 min (A) or the time indicated (C). At the end of glucose stimulation, secreted insulin concentrations were measured by ELISA and normalized by cellular protein content. Knock-down efficacy was determined by Western blot using anti-DOC2b antibody (B). Values are mean  $\pm$  SD from three independent experiments.

and translocated to the plasma membrane in response to high glucose (Fig. 2A and B). Interestingly, this translocation was intracellular calcium dependent manner. Glucose induced interaction between DOC2b and syntaxin4, but not syntaxin1 (Fig. 3). Finally, we showed that overexpression of DOC2b increased and silencing of DOC2b decreased glucose-induced insulin secretion (Fig. 4), suggesting the regulatory role of DOC2b on insulin secretion. These data were consistent with the aforementioned hypothesis that DOC2b positively regulates insulin secretion in  $\beta$ -cells.

One of the key findings of this study is the time scale of the regulation by DOC2b. As shown in Fig. 4C, DOC2b silencing did not affect the insulin secretion during the first 7 min after exposure to glucose. In contrast, DOC2b silencing apparently decreased the delayed (~60 min) insulin secretion. These data were consistent with the slow time course of DOC2b translocation to plasma membrane, suggesting the role of second-phase specific insulin secretion. To date, there are no reports on SNARE regulators for the second-

phase insulin secretion. These results were supported by the observation that DOC2b has no effects on KCl-stimulated insulin secretion (Fig. 4A and C), the first-phase specific secretagogue. Furthermore, in agreement with the report that syntaxin1 mediates first-phase specific insulin secretion [12], our observation that DOC2b specifically binds to syntaxin4, but not syntaxin1 (Fig. 3A and C), is consistent with its role on the second-phase release of insulin.

Another interesting observation in this study is the essential role of  $[\text{Ca}^{2+}]_i$  in glucose induced DOC2b translocation (Fig. 2A). DOC2b binding to syntaxin4 is also  $[\text{Ca}^{2+}]_i$  dependent (also in [27]). Ke et al. reported that DOC2b did not interact with syntaxin4 in pancreatic  $\beta$ -cells [34]. This apparent discrepancy must be attributable to the different experiment conditions. They performed their experiments using a buffer without  $\text{Ca}^{2+}$ . DOC2b has tandem C2 domains and several  $\text{Ca}^{2+}$  binding sites, and is structurally similar to the well-known calcium sensor synaptotagmins,

suggesting that  $[Ca^{2+}]_i$  might be necessary for proper function of DOC2b.

In conclusion, our results allow us to draw the following two conclusions. First, DOC2b was translocated to plasma membrane and interacted with syntaxin4 upon high-glucose stimulation in  $[Ca^{2+}]_i$  dependent manner. Second, DOC2b regulates glucose induced delayed insulin secretion in MIN6 cells. In summary, our data suggest that DOC2b may be a SNARE regulator for the second-phase secretion of insulin.

### Acknowledgments

We thank Dr. R.R. Duncan for the DOC2a, -b constructs. We are very grateful to Drs. A. Yanai and K. Shinoda (Yamaguchi University Graduate School of Medicine, Yamaguchi, Japan) for support on Immunoelectron microscopy. We also thank Ms. Y. Kora for her technical support. This work partly supported by Grants-in-Aid for Scientific Research from the Ministry of Education, Culture, Sports, Science and Technology of Japan to M.E. and Y.T., and from Takeda Scientific Foundation to M.E.

### Appendix A. Supplementary data

Supplementary data associated with this article can be found, in the online version, at doi:10.1016/j.bbrc.2009.04.133.

### References

- [1] D.L. Curry, L.L. Bennett, G.M. Grodsky, Dynamics of insulin secretion by the perfused rat pancreas, *Endocrinology* 83 (1968) 572–584.
- [2] J.C. Henquin, M.A. Ravier, M. Nenquin, J.C. Jonas, P. Gilon, Hierarchy of the  $\beta$ -cell signals controlling insulin secretion, *Eur. J. Clin. Invest.* 33 (2003) 742–750.
- [3] S.G. Straub, G.W. Sharp, Glucose-stimulated signaling pathways in biphasic insulin secretion, *Diabetes Metab. Res. Rev.* 18 (2002) 451–463.
- [4] S.H. Gerber, T.C. Südhof, Molecular determinants of regulated exocytosis, *Diabetes* 51 (2002) S3–S11.
- [5] P. Rorsman, E. Renström, Insulin granule dynamics in pancreatic beta cells, *Diabetologia* 46 (2003) 1029–1045.
- [6] M. Gemva, P. Gilon, J.C. Henquin, Evidence that glucose can control insulin release independently from its action on ATP-sensitive  $K^+$  channels in mouse B cells, *J. Clin. Invest.* 89 (1992) 1288–1295.
- [7] T. Aizawa, M. Komatsu, N. Asanuma, Y. Sato, G.W.G. Sharp, Glucose action “beyond ionic events” in the pancreatic  $\beta$  cell, *Trend Pharmacol. Sci.* 19 (1998) 496–499.
- [8] M.B. Wheeler, L. Sheu, M. Ghai, A. Bouquillon, G. Grondin, U. Weller, A.R. Beaudoin, M.K. Bennett, W.S. Trimble, H.Y. Gaisano, Characterization of SNARE protein expression in beta cell lines and pancreatic islets, *Endocrinology* 137 (1996) 1340–1348.
- [9] G. Jacobsson, A.J. Bean, R.H. Scheller, L. Junnti-Berggren, J.T. Deeney, P.O. Berggren, B. Meister, Identification of synaptic proteins and their isoform mRNAs in compartments of pancreatic endocrine cells, *Proc. Natl. Acad. Sci. USA* 91 (1994) 12487–12491.
- [10] T. Saito, S. Okada, E. Yamada, K. Ohshima, H. Shimizu, K. Shimomura, M. Sato, J.E. Pessin, M. Mori, Syntaxin 4 and Synip (syntaxin 4 interacting protein) regulate insulin secretion in the pancreatic beta HC-9 cell, *J. Biol. Chem.* 278 (2003) 36718–36725.
- [11] B.A. Spurlin, D.C. Thurmond, Syntaxin 4 facilitates biphasic glucose-stimulated insulin secretion from pancreatic beta-cells, *Mol. Endocrinol.* 20 (2006) 183–193.
- [12] M. Ohara-Imaizumi, T. Fujiwara, Y. Nakamichi, T. Okamura, Y. Akimoto, J. Kawai, S. Matsushima, H. Kawakami, T. Watanabe, K. Akagawa, S. Nagamatsu, Imaging analysis reveals mechanistic differences between first- and second-phase insulin exocytosis, *J. Cell Biol.* 177 (2007) 695–705.
- [13] S. Nagamatsu, T. Fujiwara, Y. Nakamichi, T. Watanabe, H. Katahira, H. Sawa, K. Akagawa, Expression and functional role of syntaxin 1/HPC-1 in pancreatic beta cells. Syntaxin 1A, but not 1B, plays a negative role in regulatory insulin release pathway, *J. Biol. Chem.* 271 (1996) 1160–1165.
- [14] R. Kuliawat, E. Kalinina, J. Bock, L. Fricker, T.E. McGraw, S.R. Kim, J. Zhong, R. Scheller, P. Arvan, Syntaxin-6 SNARE involvement in secretory and endocytic pathways of cultured pancreatic beta-cells, *Mol. Biol. Cell* 15 (2004) 1690–1701.
- [15] C.E. Kiraly-Borri, A. Morgan, R.D. Burgoyne, U. Weller, C.B. Wollheim, J. Lang, Soluble N-ethylmaleimide-sensitive-factor attachment protein and N-ethylmaleimide-insensitive factors are required for  $Ca^{2+}$ -stimulated exocytosis of insulin, *Biochem. J.* 314 (1996) 199–203.
- [16] R. Regazzi, C.B. Wollheim, J. Lang, J.M. Theler, O. Rossetto, C. Montecucco, K. Sadoul, U. Weller, M. Palmer, B. Thorens, VAMP-2 and cellubrevin are expressed in pancreatic beta-cells and are essential for  $Ca^{2+}$ - but not for GTP gamma S-induced insulin secretion, *EMBO J.* 14 (1995) 2723–2730.
- [17] E.R. Chapman, Synaptotagmin: a  $Ca^{2+}$  sensor that triggers exocytosis?, *Nat. Rev. Mol. Cell Biol.* 3 (2002) 498–508.
- [18] R. Jahn, T. Lang, T.C. Südhof, Membrane fusion, *Cell* 112 (2003) 519–533.
- [19] Z. Gao, J. Reavey-Cantwell, R.A. Young, P. Jegier, B.A. Wolf, Synaptotagmin III/ VII isoforms mediate  $Ca^{2+}$ -induced insulin secretion in pancreatic islet beta-cells, *J. Biol. Chem.* 275 (2000) 36079–36085.
- [20] M. Iezzi, G. Kouri, M. Fukuda, C.B. Wollheim, Synaptotagmin V and IX isoforms control  $Ca^{2+}$ -dependent insulin exocytosis, *J. Cell Sci.* 117 (2004) 3119–3127.
- [21] A. Gut, C.E. Kiraly, M. Fukuda, K. Mikoshiba, C.B. Wollheim, J. Lang, Expression and localisation of synaptotagmin isoforms in endocrine beta-cells: their function in insulin exocytosis, *J. Cell Sci.* 114 (2001) 1709–1716.
- [22] S. Orita, T. Sasaki, A. Naito, R. Komuro, T. Ohtsuka, M. Maeda, H. Suzuki, H. Igarashi, Y. Takai, Doc2: a novel brain protein having two repeated C2-like domains, *Biochem. Biophys. Res. Commun.* 206 (1995) 439–448.
- [23] R.R. Duncan, M.J. Shipston, R.H. Chow, Double C2 protein. A review, *Biochimie* 82 (2000) 421–426.
- [24] K. Fujimoto, T. Shibasaki, N. Yokoi, Y. Kashima, M. Matsumoto, T. Sasaki, N. Tajima, T. Iwanaga, S. Seino, Piccolo a  $Ca^{2+}$  sensor in pancreatic beta-cells. Involvement of cAMP-GEFII.Rim2. Piccolo complex in cAMP-dependent exocytosis, *J. Biol. Chem.* 277 (2002) 50497–50502.
- [25] F.F. Dai, Y. Zhang, Y. Kang, Q. Wang, H.Y. Gaisano, K.H. Braunewell, C.B. Chan, M.B. Wheeler, The neuronal  $Ca^{2+}$  sensor protein visinin-like protein-1 is expressed in pancreatic islets and regulates insulin secretion, *J. Biol. Chem.* 281 (2006) 21942–21953.
- [26] N. Fukuda, M. Emoto, Y. Nakamori, A. Taguchi, S. Okuya, Y. Tanizawa, DOC2b regulates GLUT4 vesicle Fusion in 3T3-L1 adipocytes, *Diabetes* 54 (2005) A71.
- [27] N. Fukuda, M. Emoto, Y. Nakamori, A. Taguchi, S. Miyamoto, S. Uraki, Y. Oka, Y. Tanizawa, DOC2B: a novel syntaxin4 binding protein mediating insulin-regulated GLUT4-vesicle fusion in adipocytes, *Diabetes* 58 (2009) 377–384.
- [28] M. Sakurada, A. Kanatsuka, T. Saitoh, H. Makino, K. Yamamura, J. Miyazaki, M. Kikuchi, S. Yoshida, Relation between glucose-stimulated insulin secretion and intracellular calcium accumulation studied with a superfusion system of a glucose-responsive pancreatic beta-cell line MIN6, *Endocrinology* 132 (1993) 2659–2665.
- [29] T. Funakoshi, A. Yanai, K. Shinoda, M.M. Kawano, Y. Mizukami, G protein-coupled receptor 30 is an estrogen receptor in the plasma membrane, *Biochem. Biophys. Res. Commun.* 346 (2006) 904–910.
- [30] M. Fukuda, C. Saegusa, E. Kanno, K. Mikoshiba, The C2A domain of double C2 protein gamma contains a functional nuclear localization signal, *J. Biol. Chem.* 276 (2001) 24441–24444.
- [31] A.J. Groffen, E.C. Brian, J.J. Dudok, J. Kampmeijer, R.F. Toonen, M. Verhage,  $Ca^{2+}$ -induced recruitment of the secretory vesicle protein DOC2B to the target membrane, *J. Biol. Chem.* 279 (2004) 23740–23747.
- [32] A.J. Groffen, R. Friedrich, E.C. Brian, U. Ashery, M. Verhage, DOC2A and DOC2B are sensors for neuronal activity with unique calcium-dependent and kinetic properties, *J. Neurochem.* 97 (2006) 818–833.
- [33] R.B. Sutton, B.A. Davletov, A.M. Berghuis, T.C. Südhof, S.R. Sprang, Structure of the first C2 domain of synaptotagmin I: a novel  $Ca^{2+}$ /phospholipid-binding fold, *Cell* 80 (1995) 929–938.
- [34] B. Ke, E. Oh, D.C. Thurmond, Doc2beta is a novel Munc18c-interacting partner and positive effector of syntaxin 4-mediated exocytosis, *J. Biol. Chem.* 282 (2007) 21786–21797.

# Activation of AMP-activated Protein Kinase Suppresses Oxidized Low-density Lipoprotein-induced Macrophage Proliferation\*

Received for publication, June 1, 2009, and in revised form, October 15, 2009. Published, JBC Papers in Press, October 20, 2009, DOI 10.1074/jbc.M109.028043

Norio Ishii<sup>†1</sup>, Takeshi Matsumura<sup>†1,2</sup>, Hiroyuki Kinoshita<sup>†</sup>, Hiroyuki Motoshima<sup>†</sup>, Kanou Kojima<sup>†</sup>, Atsuyuki Tsutsumi<sup>†</sup>, Shuji Kawasaki<sup>†</sup>, Miyuki Yano<sup>†</sup>, Takafumi Senokuchi<sup>†</sup>, Tomoichiro Asano<sup>§</sup>, Takeshi Nishikawa<sup>†</sup>, and Eiichi Araki<sup>†</sup>

From the <sup>†</sup>Department of Metabolic Medicine, Graduate School of Medical Sciences, Kumamoto University, Kumamoto 860-8556 and the <sup>§</sup>Department of Medical Chemistry, Division of Molecular Medical Science, Graduate School of Biomedical Science, Hiroshima University, Hiroshima 734-8551, Japan

Macrophage-derived foam cells play important roles in the progression of atherosclerosis. We reported previously that ERK1/2-dependent granulocyte/macrophage colony-stimulating factor (GM-CSF) expression, leading to p38 MAPK/Akt signaling, is important for oxidized low density lipoprotein (Ox-LDL)-induced macrophage proliferation. Here, we investigated whether activation of AMP-activated protein kinase (AMPK) could suppress macrophage proliferation. Ox-LDL-induced proliferation of mouse peritoneal macrophages was assessed by [<sup>3</sup>H]thymidine incorporation and cell counting assays. The proliferation was significantly inhibited by the AMPK activator 5-aminoimidazole-4-carboxamide ribonucleoside (AICAR) and restored by dominant-negative AMPK $\alpha$ 1, suggesting that AMPK activation suppressed macrophage proliferation. AICAR partially suppressed Ox-LDL-induced ERK1/2 phosphorylation and GM-CSF expression, suggesting that another mechanism is also involved in the AICAR-mediated suppression of macrophage proliferation. AICAR suppressed GM-CSF-induced macrophage proliferation without suppressing p38 MAPK/Akt signaling. GM-CSF suppressed p53 phosphorylation and expression and induced Rb phosphorylation. Overexpression of p53 or p27<sup>kip</sup> suppressed GM-CSF-induced macrophage proliferation. AICAR induced cell cycle arrest, increased p53 phosphorylation and expression, and suppressed GM-CSF-induced Rb phosphorylation via AMPK activation. Moreover, AICAR induced p21<sup>cip</sup> and p27<sup>kip</sup> expression via AMPK activation, and small interfering RNA (siRNA) of p21<sup>cip</sup> and p27<sup>kip</sup> restored AICAR-mediated suppression of macrophage proliferation. In conclusion, AMPK activation suppressed Ox-LDL-induced macrophage proliferation by suppressing GM-CSF expression and inducing cell cycle

arrest. These effects of AMPK activation may represent therapeutic targets for atherosclerosis.

Macrophages are well known to be present in all stages of atherosclerosis and are considered to be fundamental to atherogenesis and the behavior of established plaques (1). Macrophages take up oxidized low density lipoprotein (Ox-LDL)<sup>3</sup> through scavenger receptor pathways and transform into foam cells *in vitro* (2). Foam cells produce various bioactive molecules, such as cytokines and growth factors, which are believed to play important roles in the development and progression of atherosclerosis (1).

One of the characteristic events in atherosclerotic lesions is the proliferation of cells, including vascular smooth muscle cells and macrophages, within arterial walls. Indeed, previous *in vivo* studies have reported that macrophages and macrophage-derived foam cells proliferate in atherosclerotic lesions (3–5). We (6–8) and others (9, 10) have shown that Ox-LDL enhances macrophage proliferation and survival *in vitro*. Therefore, it is possible that macrophage proliferation may promote the progression of atherosclerosis.

We previously reported that Ox-LDL-induced production of granulocyte/macrophage colony-stimulating factors (GM-CSFs) plays an important role in the growth signaling pathway for Ox-LDL-induced macrophage proliferation (11, 12). Moreover, we recently reported that the p38 MAPK/phosphatidylinositol 3-kinase/Akt signaling pathway is involved, at least in part, in the downstream signaling pathways after GM-CSF expression (8, 13).

AMP-activated protein kinase (AMPK) belongs to a protein kinase family that has been highly conserved throughout evolution in animals, plants, and yeast and plays major roles in cell responses to metabolic stress (14–16). AMPK is a heterotrimeric protein consisting of a catalytic  $\alpha$  subunit and regulatory  $\beta$  and  $\gamma$  subunits (17). Each  $\alpha$  and  $\beta$  subunit is encoded by two

\* This work was supported by grants-in-aid for scientific research from the Japan Society for the Promotion of Science, Japan (21591144, to T. M. and 20390259, to E. A.), a grant from the Takeda Science Foundation (to T. M.), and the Advanced Education Program for Integrated Clinical, Basic and Social Medicine, Graduate School of Medical Sciences, Kumamoto University (Support Program for Improving Graduate School Education, MEXT, Japan).

<sup>†</sup> Both authors contributed equally to this work.

<sup>2</sup> To whom correspondence should be addressed: Dept. of Metabolic Medicine, Graduate School of Medical Sciences, Kumamoto University, 1-1-1 Honjo, Kumamoto 860-8556, Japan. Tel.: 81-96-373-5169; Fax: 81-96-366-8397; E-mail: takeshim@gpo.kumamoto-u.ac.jp.

<sup>3</sup> The abbreviations used are: Ox-LDL, oxidized low density lipoprotein; ACC, acetyl-CoA carboxylase; Ad, adenovirus; AICAR, 5-aminoimidazole-4-carboxamide ribonucleoside; AMPK, AMP-activated protein kinase; DN, dominant-negative; CDKs, cyclin-dependent kinase inhibitors; ERK1/2, extracellular signal-regulated kinase 1/2; ELISA, enzyme-linked immunosorbent assay; MAPK, mitogen-activated protein kinase; SMC, smooth muscle cell; siRNA, small interfering RNA; WT, wild-type.

## AMPK Suppresses Ox-LDL-induced Macrophage Proliferation

genes ( $\alpha 1$  and  $\alpha 2$  or  $\beta 1$  and  $\beta 2$ ), whereas the  $\gamma$  subunit is encoded by three genes ( $\gamma 1$ ,  $\gamma 2$ , and  $\gamma 3$ ). The protein is activated in response to increased ratios of AMP to ATP within the cell and therefore acts as an efficient sensor for the cellular energy state. AMP activates AMPK by direct allosteric activation and by protecting dephosphorylation of threonine residue (Thr-172) within the activation domain of the  $\alpha$  subunit by inhibiting protein phosphatase 2C $\alpha$  (17, 18). One of the downstream targets of AMPK is the regulation of lipid metabolism. It is well known that AMPK directly phosphorylates and inactivates acetyl-CoA carboxylase (ACC), thereby suppressing malonyl-CoA production. The reduction in malonyl-CoA accelerates the entry of long-chain acyl-CoA into mitochondria for  $\beta$ -oxidation to restore the energy balance (17). 5-Aminoimidazole-4-carboxamide ribonucleoside (AICAR) is a well known activator of AMPK. AICAR is transported into cells through adenosine transporters and phosphorylated by adenosine kinase (19) to form 5-aminoimidazole-4-carboxamide-1- $\beta$ -ribofuranosyl-5'-monophosphate, which mimics the stimulatory action of AMP on AMPK (20). Recently, we (21) and others (22) reported that the proliferation of vascular smooth muscle cells (SMCs) is suppressed by activation of AMPK. On the other hand, Jhun *et al.* (23) reported that AICAR suppresses lipopolysaccharide-induced tumor necrosis factor- $\alpha$  expression in RAW264.7 murine macrophages. Therefore, AMPK activation may protect against the acceleration of atherosclerosis by suppressing SMC proliferation and inactivating macrophages. However, there is no further evidence regarding the issue of whether AMPK activation can suppress atherosclerotic events in macrophages, such as their proliferation.

In the present study, we investigated the effects of AMPK activation on Ox-LDL-induced macrophage proliferation. We found that AICAR-mediated AMPK activation suppressed Ox-LDL-induced macrophage proliferation by suppressing GM-CSF expression and inducing cell cycle arrest.

### EXPERIMENTAL PROCEDURES

**Materials**—AICAR was purchased from Toronto Research Chemicals (North York, Ontario, Canada). Antibodies against the total proteins of AMPK $\alpha$ , Rb, p53, and p21<sup>cip</sup> and phosphospecific antibodies against ACC (Ser-79), AMPK $\alpha 1$  (Thr-172), p53 (Ser-15), Rb (Ser-807/811), ERK1/2, p38 MAPK, and Akt were obtained from Cell Signaling Technology (Beverly, MA). Antibodies against the total proteins of ERK1/2, p38 MAPK, Akt, p27<sup>kip</sup>, and  $\beta$ -actin were purchased from Santa Cruz Biotechnology (Santa Cruz, CA). All other chemicals were of the best grade available from commercial sources.

**Lipoprotein Preparation**—Human LDL ( $d = 1.019$ – $1.063$  g/ml) was isolated by ultracentrifugation from plasma samples obtained from consenting normolipidemic subjects after an overnight fast (7). LDL was dialyzed against 0.15 M NaCl and 1 mM EDTA (pH 7.4). Ox-LDL was prepared by incubation of LDL with 5  $\mu$ M CuSO<sub>4</sub> for 20 h at 37 °C, followed by the addition of 1 mM EDTA and cooling (7). The protein concentrations were determined using the BCA protein assay reagent (Pierce). The endotoxin level in the prepared Ox-LDL was <1 pg/ $\mu$ g protein, as measured using a Toxicolor System (Seikagaku Corp., Tokyo, Japan) (7).

**Cell Cultures**—The experimental protocol was approved by the Ethics Review Committee for Animal Experimentation of Kumamoto University. Peritoneal macrophages were collected from anesthetized male C3H/He mice (25–30 g) by peritoneal lavage with 8 ml of phosphate-buffered saline, centrifuged at 200  $\times g$  for 5 min, resuspended in medium A (RPMI 1640 medium (Nissui Seiyaku Co., Tokyo, Japan)) supplemented with 10% fetal calf serum (Invitrogen), 0.1 mg/ml streptomycin, and 100 units/ml penicillin) and incubated in appropriate tissue culture plates for 90 min (7). More than 98% of the adherent cells were considered to be macrophages based on four criteria, as described previously (24, 25).

**Infection with Adenoviral Vectors**—Adenoviruses expressing wild-type (WT)-AMPK $\alpha 1$  (Ad-AMPK $\alpha 1$ ) and dominant-negative (DN)-AMPK $\alpha 1$  (Ad-DN-AMPK $\alpha 1$ ), which serves as a nonphosphorylatable T172A mutant of the AMPK $\alpha 1$ -subunit (26) and contains a *c-myc* tag at the NH<sub>2</sub> terminus, were used as described previously (27). An adenovirus vector that expresses WT p53 (Ad-p53) was kindly gifted from Dr. Shinji Ishikawa (Department of Gastroenterological Surgery, Graduate School of Medical Sciences, Kumamoto University, Kumamoto, Japan). Mouse peritoneal macrophages were infected with the indicated adenoviral vectors at a multiplicity of infection of  $\sim 100$ , as described previously (28) and allowed to recover in medium A for 2 h. These conditions conferred expression of LacZ using adenoviruses expressing LacZ (Ad-LacZ) as a marker gene in nearly 100% of the transfected cells.

**Transfection of Plasmid**—An expression plasmid of human p27<sup>kip</sup> (pcDNA3FLAG-hp27) was kindly gifted from Dr. Masaki Matsumoto (Department of Molecular and Cellular Biology, Medical Institute of Bioregulation, Kyushu University, Fukuoka, Japan). Mouse peritoneal macrophages ( $2 \times 10^6$  cells/well) were transfected with pcDNA3FLAG-hp27 using Lipofectamine 2000 (Invitrogen, Japan, K.K. Tokyo, Japan) and incubated for 4 h. Then, the medium was removed, and cells were resuspended with medium A (29). After a 24-h incubation, cells were treated with recombinant GM-CSF, and Western blot assay and tritiated thymidine incorporation assay were performed as described below.

**Transfection of siRNA**—The siRNAs against p21<sup>cip</sup> and p27<sup>kip</sup> and an irrelevant 21-nucleotide siRNA duplex as a control were purchased from Santa Cruz Biotechnology. Mouse peritoneal macrophages ( $2 \times 10^6$  cells/well) were transfected with the siRNA of p21<sup>cip</sup>, p27<sup>kip</sup>, or control using Lipofectamine 2000 (Invitrogen) as described above.

**Tritiated Thymidine Incorporation and Cell Counting Assays**—Macrophage monolayers ( $2 \times 10^6$  cells/well) were cultured in 24-well tissue culture plates (15.5 mm in diameter; Corning Glass Works, Corning, NY) in the presence of various effectors for 6 days. For thymidine incorporation assays, the cells were incubated with 1  $\mu$ Ci/ml [<sup>3</sup>H]thymidine for 18 h before the termination of the experiments. Tritiated thymidine incorporation assays were performed as described previously (7). For cell counting assays, cultured cells were lysed in 1% (w/v) Triton X-100, and naphthol blue-black-stained nuclei were counted in a hemocytometer as described previously (11, 13).



## AMPK Suppresses Ox-LDL-induced Macrophage Proliferation

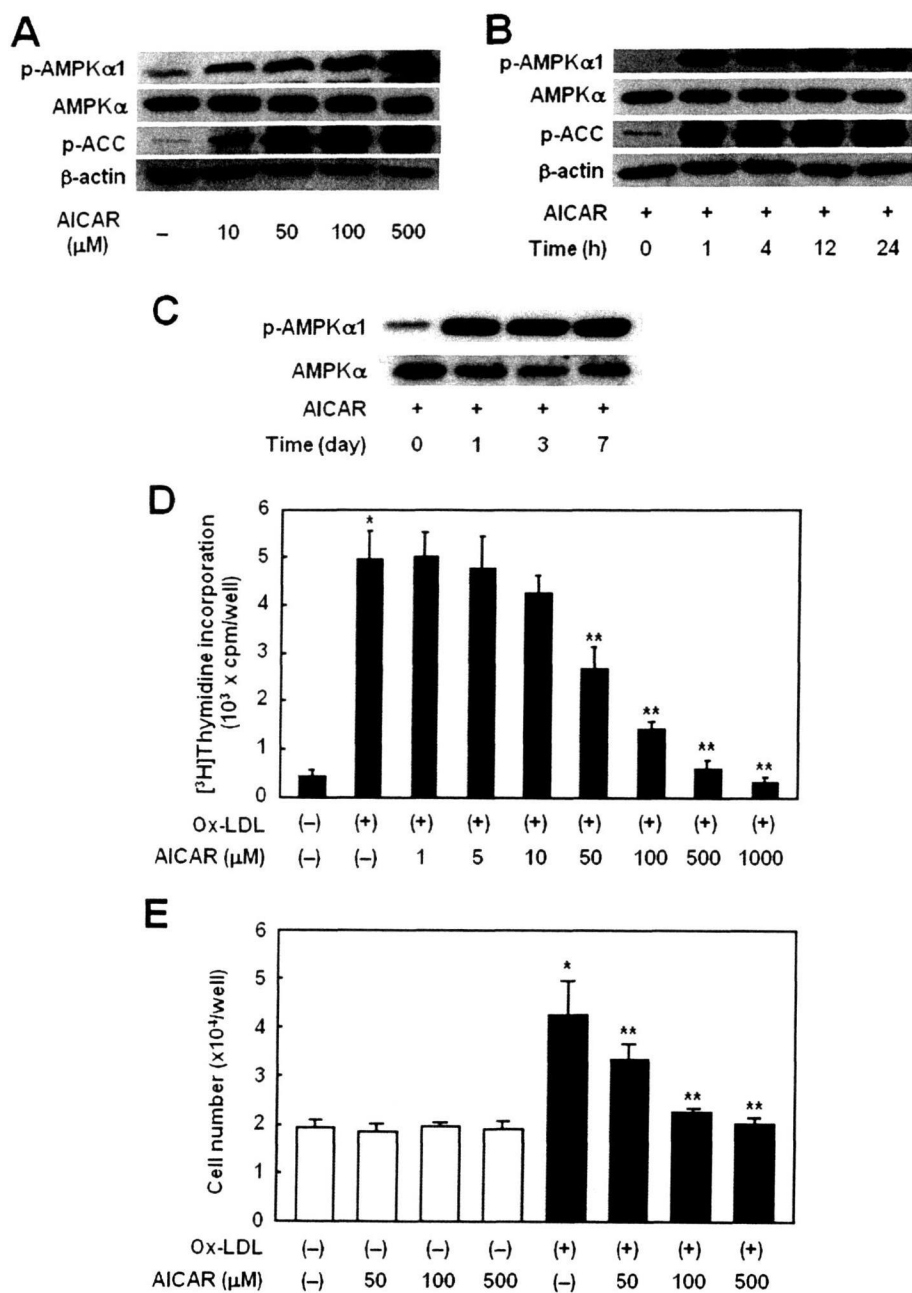


**FIGURE 1. Ox-LDL-induced macrophage proliferation is suppressed by AICAR.** A, B, and C, mouse peritoneal macrophages were incubated with the indicated concentrations of AICAR for 1 h (A) or incubated with 100  $\mu$ M AICAR for the indicated periods of time (B and C). Protein samples were immunoblotted with anti-phospho-AMPK $\alpha$ 1 (p-AMPK $\alpha$ 1), anti-AMPK $\alpha$ 1, anti-phospho-ACC (p-ACC), or anti- $\beta$ -actin antibodies. The data are representative of four separate experiments. D and E, macrophages were pretreated with the indicated concentrations of AICAR for 1 h and then cultured with 20  $\mu$ g/ml Ox-LDL for 6 days. [<sup>3</sup>H]Thymidine incorporation assays (D) and cell counting assays (E) were performed. Data represent the means  $\pm$  S.E. of four separate experiments. \*,  $p < 0.01$ , compared with untreated cells. \*\*,  $p < 0.01$ , compared with cells incubated with Ox-LDL alone.

**Western Blot Analysis**—Macrophages ( $2 \times 10^6$  cells/well) were incubated with various effectors, and whole cell lysates were purified as described previously (8). The protein concentrations were determined using the Micro BCA protein assay reagent (Pierce). Samples were separated by electrophoresis in 10% polyacrylamide gels and transferred to nitrocellulose membranes (Bio-Rad). The membranes were incubated with

appropriate primary antibodies at a dilution of 1:1,000 for 2 h. After washing, the membranes were stained with a horseradish peroxidase-conjugated goat anti-rabbit secondary antibody (Santa Cruz Biotechnology) (8). Immunoreactive bands were quantified using National Institutes of Health Image analysis software (8).

**Enzyme-linked Immunosorbent Assay (ELISA) for GM-CSF**—Macrophages ( $5 \times 10^6$  cells/plate) were cultured with various effectors, followed by the addition of 20  $\mu$ g/ml Ox-LDL. After 4 h of incubation, the media were collected, and the GM-CSF protein concentrations were determined as described previously (10).

**Cell Cycle Analysis by Flow Cytometry**—Macrophages ( $1 \times 10^6$  cells/well) were incubated with various effectors for 48 h (apoptosis assays) or 96 h (cell cycle analyses). The cells were then fixed with 70% ethanol, treated with RNase A (0.25 mg/ml), and stained with propidium iodide (0.02 mg/ml). The fractions of cells present in the different cell cycle phases ( $G_0/G_1$ , S, and  $G_2/M$ ) were determined by flow cytometry using a FACStar flow cytometer (BD Biosciences) and the Modifit software (Verity House, Topsham, ME) (21).

**Apoptosis Assay**—Macrophages ( $1 \times 10^5$  cells/well) were incubated with various effectors for 48 h and then subjected to quantification of cytoplasmic histone-associated DNA fragments using a cell death detection ELISA kit (Roche Applied Science). In addition, the percentages of sub- $G_0/G_1$  cells were analyzed by flow cytometry as described above.

**Statistical Analysis**—All data were expressed as the mean  $\pm$  S.E. Differences between groups were examined for statistical significance

by one-factor analysis of variance. Values of  $p < 0.01$  were considered to indicate a statistically significant difference.

## RESULTS

**AICAR Inhibits Ox-LDL-induced Macrophage Proliferation**—It has been reported that mouse peritoneal macrophages express high levels of AMPK $\alpha$ 1 but express low levels of

## AMPK Suppresses Ox-LDL-induced Macrophage Proliferation

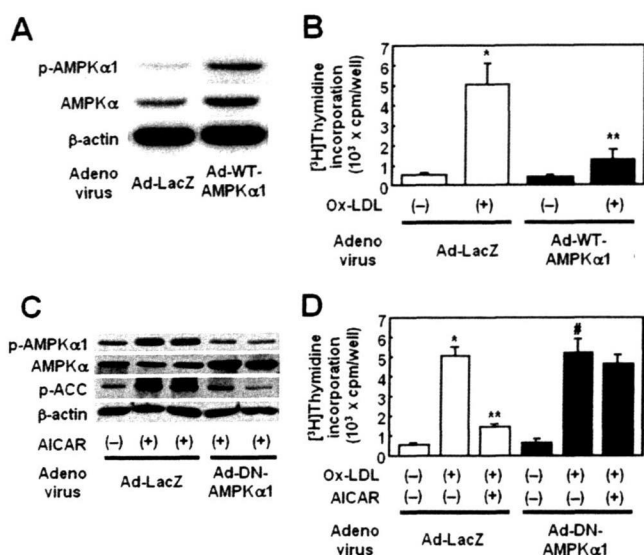


**FIGURE 2. AICAR suppresses Ox-LDL-induced macrophage proliferation by AMPK activation.** A–D, macrophages were infected with adenoviral vectors containing LacZ (Ad-LacZ), wild-type AMPK $\alpha$ 1 (Ad-WT-AMPK $\alpha$ 1) (A and B) or dominant-negative AMPK $\alpha$ 1 (Ad-DN-AMPK $\alpha$ 1) (C and D), cultured for 48 h, and incubated with or without 100  $\mu$ M AICAR for 1 h. A and C, protein samples were immunoblotted with anti-phospho-AMPK $\alpha$ 1 (p-AMPK $\alpha$ 1), anti-AMPK $\alpha$ 1, anti-phospho-ACC (p-ACC), or anti- $\beta$ -actin antibodies. The data are representative of four experiments. B and D, cells were cultured with 20  $\mu$ g/ml Ox-LDL for 6 days and subjected to [<sup>3</sup>H]thymidine incorporation assays. Data represent the means  $\pm$  S.E. of four separate experiments. \*,  $p < 0.01$ , compared with untreated cells infected with Ad-LacZ. \*\*,  $p < 0.01$ , compared with Ad-LacZ-infected cells incubated with Ox-LDL alone. #,  $p < 0.01$ , compared with untreated cells infected with Ad-DN-AMPK $\alpha$ 1.

AMPK $\alpha$ 2 (23). Therefore, we focused on AMPK $\alpha$ 1 and investigated whether AICAR could induce AMPK $\alpha$ 1 activation in mouse peritoneal macrophages. AICAR phosphorylated AMPK $\alpha$ 1 and ACC, one of the target molecules of AMPK, in dose-dependent manners (Fig. 1A). Moreover, our time course experiments revealed that AICAR-induced phosphorylation of AMPK $\alpha$ 1 and ACC was observed as early as 1 h, which sustained until 7 days (Fig. 1, B and C). These results confirmed that AICAR activated AMPK $\alpha$ 1 and its downstream signals in macrophages.

Next, we examined the effects of AICAR on Ox-LDL-induced macrophage proliferation. Ox-LDL (20  $\mu$ g/ml) significantly increased [<sup>3</sup>H]thymidine incorporation into macrophages (Fig. 1D), as previously reported (6–8, 12). Pretreatment with AICAR at concentrations of 50  $\mu$ M or higher suppressed the Ox-LDL-induced increase in [<sup>3</sup>H]thymidine incorporation in a dose-dependent manner (Fig. 1D). Cell counting assays confirmed that the Ox-LDL-induced increase in cell number was suppressed by AICAR (Fig. 1E).

To clarify the involvement of AMPK activation in AICAR-mediated suppression of macrophage proliferation, we examined the effects of WT-AMPK $\alpha$ 1 and DN-AMPK $\alpha$ 1 on macrophage proliferation. Expression of WT-AMPK $\alpha$ 1 by an adenovirus vector caused ~2-fold increases in total AMPK expression and AMPK $\alpha$ 1 phosphorylation (Fig. 2A) and suppressed Ox-LDL-induced macrophage proliferation (Fig. 2B). Moreover, overexpression of DN-AMPK $\alpha$ 1 suppressed the phosphorylation of AMPK $\alpha$ 1 and ACC (Fig. 2C) and restored AICAR-mediated suppression of macrophage proliferation

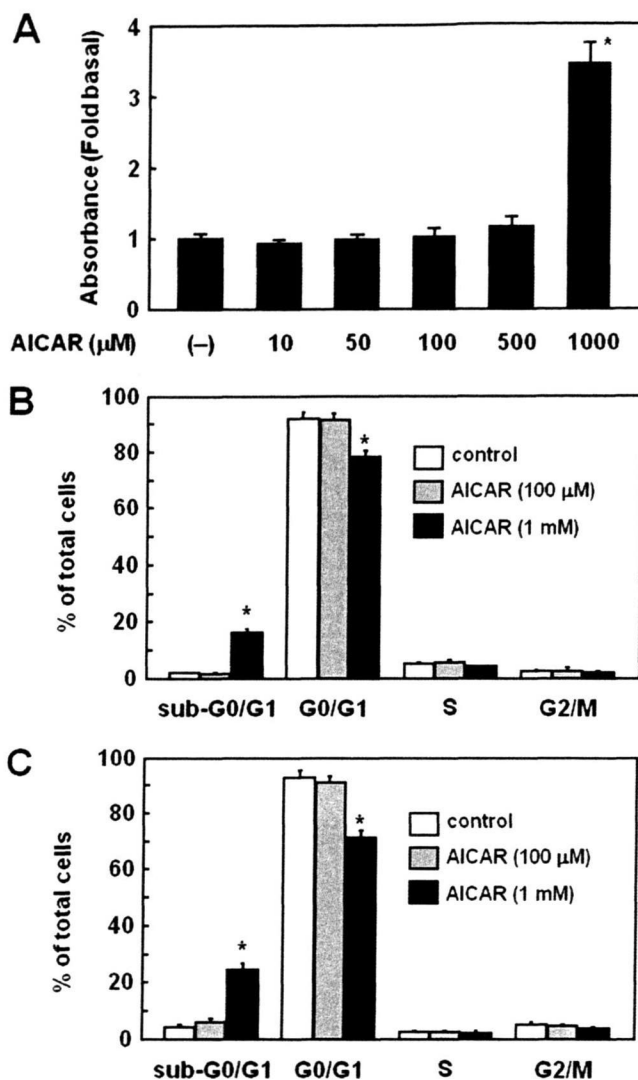


**FIGURE 3. Effects of AICAR on apoptosis of macrophages.** A–C, macrophages were incubated with the indicated concentrations of AICAR for 48 h (A and B) or 7 days (C). Apoptosis was quantified by measuring the amounts of cellular DNA fragmentation using a cell death detection ELISA kit (A) or the percentages of sub-G<sub>0</sub>/G<sub>1</sub> cells using flow cytometry (B and C). \*,  $p < 0.01$ , compared with untreated cells.

(Fig. 2D), suggesting that AICAR-mediated suppression of macrophage proliferation was caused by activation of AMPK.

**AICAR-induced Macrophage Apoptosis Is Not the Main Mechanism for the Suppression of Macrophage Proliferation**—It has been reported that activation of AMPK induces apoptosis in human B-cell chronic lymphocytic leukemia cells (30) and human neuroblastoma cells (31). Therefore, we examined the effects of AICAR on macrophage apoptosis. At 1,000  $\mu$ M, AICAR induced macrophage apoptosis (Fig. 3A). However, AICAR at concentrations of 500  $\mu$ M or lower, which can suppress macrophage proliferation, did not induce macrophage apoptosis (Fig. 3A). To obtain further evidence, the percentages of sub-G<sub>0</sub>/G<sub>1</sub> cells were quantified by fluorescence-activated cell sorter analysis using propidium iodide staining (Fig. 3, B and C). Neither 10  $\mu$ M nor 100  $\mu$ M AICAR increased the percentage of sub-G<sub>0</sub>/G<sub>1</sub> cells in both 48 h and 7 days incubation,

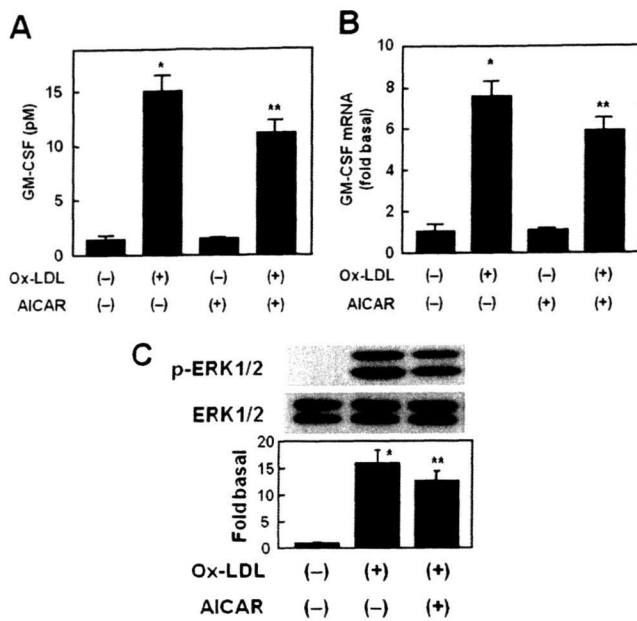


**FIGURE 4. Effects of AICAR on Ox-LDL-induced GM-CSF production and ERK1/2 phosphorylation.** *A* and *B*, macrophages were pretreated with 100  $\mu$ M AICAR for 1 h and then cultured with 20  $\mu$ g/ml Ox-LDL for 4 h (*A*) or 1 h (*B*). *A*, the levels of GM-CSF in the culture media were determined by ELISA. *B*, the mRNA expression levels of GM-CSF and  $\beta$ -actin were evaluated by real-time reverse transcription-PCR. Data represent the means  $\pm$  S.E. of four separate experiments. \*,  $p < 0.01$ , compared with untreated cells. \*\*,  $p < 0.01$ , compared with cells incubated with Ox-LDL alone. *C*, macrophages were pretreated with 100  $\mu$ M AICAR for 1 h and then cultured with 20  $\mu$ g/ml Ox-LDL for 30 min. Protein samples were immunoblotted with anti-phospho-ERK1/2 (*p*-ERK1/2) and anti-ERK1/2 (ERK1/2) antibodies. Data represent the means  $\pm$  S.E. of four separate experiments. \*,  $p < 0.01$ , compared with untreated cells. \*\*,  $p < 0.01$ , compared with cells incubated with Ox-LDL alone.

whereas 1,000  $\mu$ M AICAR markedly increased the percentage of sub- $G_0/G_1$  cells (Fig. 3, *B* and *C*). Therefore, mechanisms other than apoptosis are involved in the suppression of macrophage proliferation by low concentrations of AICAR.

**AICAR Partially Suppresses Ox-LDL-induced GM-CSF Expression**—We previously reported that ERK1/2-dependent GM-CSF expression is mainly involved in Ox-LDL-induced macrophage proliferation (8, 11). Therefore, we examined the effects of AICAR on Ox-LDL-induced GM-CSF expression and ERK1/2 phosphorylation. AICAR at 100  $\mu$ M, which can suppress macrophage proliferation by 85% based on the cell counting assay, slightly but significantly suppressed Ox-LDL-induced GM-CSF protein (Fig. 4*A*) and mRNA (Fig. 4*B*) expressions by 29 and 25%, respectively. Moreover, 100  $\mu$ M AICAR also suppressed Ox-LDL-induced ERK1/2 phosphorylation by 22% (Fig. 4*C*). These results suggested that suppression of ERK1/2-dependent GM-CSF expression was partially, but not mainly, involved in the AICAR-mediated suppression of macrophage proliferation.

**AICAR Suppresses GM-CSF-induced Macrophage Proliferation**—To clarify possible mechanisms other than GM-CSF production for the AICAR-mediated suppression of macrophage proliferation, we examined the effects of AICAR on GM-CSF-induced macrophage proliferation. At 10 pM, GM-CSF significantly increased [ $^3$ H]thymidine incorporation into macrophages (Fig. 5*A*), as previously reported (8). Pretreatment with AICAR at concentrations of 50  $\mu$ M or higher dose-dependently

suppressed the GM-CSF-induced increase in [ $^3$ H]thymidine incorporation (Fig. 5*A*). Cell counting assays confirmed that the GM-CSF-induced increase in cell number was suppressed by AICAR (Fig. 5*B*). Overexpression of WT-AMPK $\alpha$ 1 suppressed GM-CSF-induced macrophage proliferation (Fig. 5*C*). Moreover, overexpression of DN-AMPK $\alpha$ 1 restored AICAR-mediated suppression of macrophage proliferation (Fig. 5*D*). These results suggested that AICAR-mediated AMPK activation suppressed GM-CSF-induced macrophage proliferation.

**AICAR Induces Cell Cycle Arrest without Suppression of p38MAPK/Akt Signal**—We previously reported that GM-CSF expression is involved in Ox-LDL-induced macrophage proliferation (8, 11). Moreover, among the downstream signals of GM-CSF release, p38 MAPK and its subsequent signaling molecules phosphatidylinositol 3-kinase and Akt are mainly involved in Ox-LDL-induced macrophage proliferation. Therefore, we investigated the effects of AICAR on GM-CSF-induced activation of p38 MAPK and Akt. GM-CSF increased the phosphorylation of p38 MAPK and Akt (Fig. 6*A*), as reported previously (8). Surprisingly, treatment with AICAR alone also induced phosphorylation of p38 MAPK and Akt, and AICAR enhanced the GM-CSF-induced phosphorylation of p38 MAPK and Akt (Fig. 6*A*), suggesting that p38 MAPK/Akt signaling was not the main target for AICAR-mediated suppression of macrophage proliferation.

Next, we investigated the effects of AICAR on GM-CSF-induced cell cycle progression by flow cytometry. Compared with control cells treated with GM-CSF, AICAR significantly increased the percentage of cells in  $G_0/G_1$  phase (from 80.3  $\pm$  1.5% to 93.4  $\pm$  1.8%) and decreased the percentages in S phase (from 13.2  $\pm$  0.9% to 6.1  $\pm$  0.5%) and  $G_2/M$  phase (from 7.2  $\pm$  0.7% to 2.5  $\pm$  0.3%) (Fig. 6*B*), suggesting that AICAR induced  $G_1$  arrest in the proliferating macrophages.

**AICAR Increases the Expression of p21<sup>cip</sup> and p27<sup>kip</sup>, Thereby Suppressing Macrophage Proliferation**—Based on the above findings, we investigated the effects of AICAR on the phosphorylation and expression of p53, which is a suppressor of cell cycle progression. Treatment with GM-CSF suppressed the phosphorylation and expression of p53 (Fig. 6, *C* and *D*). Pretreatment with AICAR restored the GM-CSF-induced suppression of phosphorylation and expression of p53, and these effects by AICAR were abrogated by the treatment with DN-AMPK $\alpha$ 1 (Fig. 6, *C* and *D*). Interestingly, treatment with AICAR alone increased the phosphorylation and expression of p53 (Fig. 6, *C* and *D*). Moreover, treatment with GM-CSF increased the phosphorylation of Rb (Fig. 6, *C* and *E*), which is a regulator of cell cycle progression, and pretreatment with AICAR suppressed this effect (*C* and *E*).

We further investigated the effects of AICAR on the expression of the cyclin-dependent kinase inhibitors (CDKIs) p21<sup>cip</sup> and p27<sup>kip</sup>. Treatment with GM-CSF decreased p21<sup>cip</sup> expression (Fig. 6, *C* and *D*). Pretreatment with AICAR rescued the GM-CSF-mediated suppression of p21<sup>cip</sup> expression, and these effects by AICAR were abrogated by the treatment with DN-AMPK $\alpha$ 1 (Fig. 6, *C* and *D*). On the other hand, treatment with GM-CSF did not affect p27<sup>kip</sup> expression (Fig. 6, *C* and *E*), whereas pretreatment with AICAR increased p27<sup>kip</sup> expression

## AMPK Suppresses Ox-LDL-induced Macrophage Proliferation

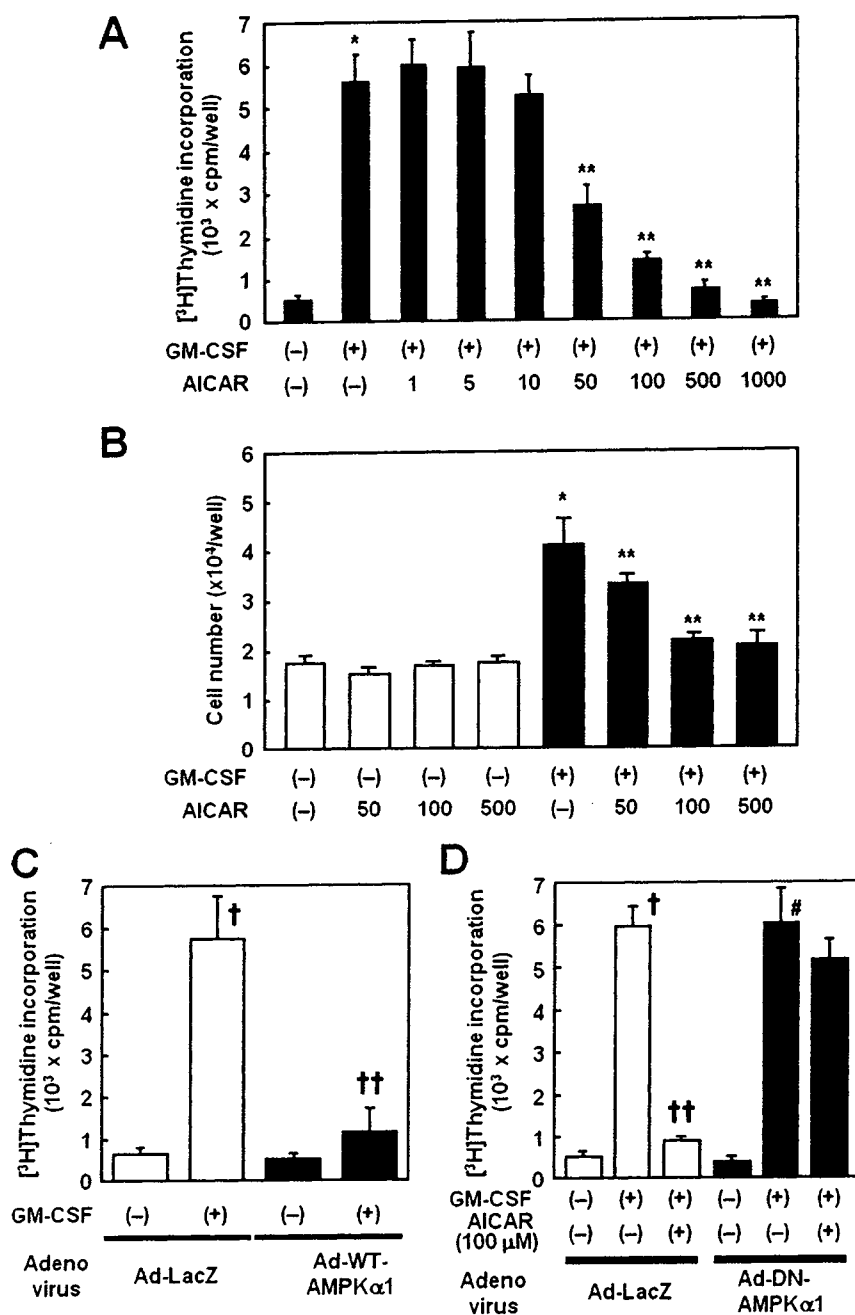


**FIGURE 5. AICAR suppresses GM-CSF-induced macrophage proliferation by AMPK activation.** A–D, macrophages were left untreated (A and B) or infected with adenoviral vectors containing LacZ (Ad-LacZ) and wild-type AMPKα1 (Ad-WT-AMPKα1) (C) or Ad-LacZ and dominant-negative AMPKα1 (Ad-DN-AMPKα1) (D) and then cultured for 48 h. After treatment with the indicated concentrations of AICAR for 1 h, the cells were cultured with 10 pM GM-CSF for 5 days. [<sup>3</sup>H]Thymidine incorporation assays (A and C) and cell counting assays (B) were performed. Data represent the means ± S.E. of four separate experiments. \*, *p* < 0.01, compared with untreated cells. \*\*, *p* < 0.01, compared with cells incubated with GM-CSF alone. †, *p* < 0.01, compared with untreated cells infected with Ad-LacZ. ††, *p* < 0.01, compared with Ad-LacZ-infected cells incubated with GM-CSF alone. #, *p* < 0.01, compared with untreated cells infected with Ad-DN-AMPKα1.

(C and E). Moreover, treatment with DN-AMPKα1 attenuated these effects by AICAR (Fig. 6, C and E). Interestingly, treatment with AICAR alone increased the expression of p21<sup>cip</sup> and p27<sup>kip</sup> (Fig. 6, C–E).

We next investigated the effects of overexpression of p21<sup>cip</sup> and p27<sup>kip</sup> on GM-CSF-induced macrophage proliferation.

Introduction of Ad-p53 increased the expression and phosphorylation of p53, increased the expression of p21<sup>cip</sup>, and suppressed GM-CSF-induced increase in [<sup>3</sup>H]thymidine incorporation into macrophages (Fig. 7, A and B). Moreover, introduction of pcDNA3FLAG-hp27 increased the expression of p27<sup>kip</sup> and suppressed GM-CSF-induced increase in [<sup>3</sup>H]thymidine incorporation (Fig. 7, C and D). Finally, we investigated the effects of siRNA for p21<sup>cip</sup> and/or p27<sup>kip</sup> on GM-CSF-induced macrophage proliferation. In comparison with the control siRNA, siRNA for p21<sup>cip</sup> and p27<sup>kip</sup> suppressed the AICAR-induced expression of p21<sup>cip</sup> and p27<sup>kip</sup>, respectively (Fig. 7, E and F). Moreover, treatment with p21<sup>cip</sup> siRNA and p27<sup>kip</sup> siRNA restored AICAR-mediated suppression of macrophage proliferation, and additive effect of the siRNAs was observed (Fig. 7G), suggesting that AICAR-mediated increase in the expression of p21<sup>cip</sup> and p27<sup>kip</sup> is involved in AICAR-mediated suppression of macrophage proliferation.

## DISCUSSION

AMPK is a serine/threonine protein kinase that serves as an energy sensor in all eukaryotic cells (14). Several studies have indicated that AMPK activation by AICAR strongly suppresses cell proliferation in hepatoma HepG2 cells (32) and mouse embryonic fibroblasts (33). Moreover, we recently reported that AMPK activation suppresses proliferation in human aortic SMCs and rabbit aortic strips (21). In the present study, we have demonstrated that AICAR-mediated AMPK activation also suppresses Ox-LDL-induced macrophage proliferation.

Activation of AMPK induces apoptosis in human B-cell chronic lymphocytic leukemia cells (30) and human neuroblastoma cells (31). Consequently, we speculated that the inhibitory effects of AMPK activation would be mediated by macrophage apoptosis. In fact, we found for the first time that 1 mM AICAR induced macrophage apoptosis. However, suppression of macrophage proliferation was still observed at low concentrations of AICAR (<1 mM). Therefore,